On the Origin of the Bolivian High and Related Circulation Features of the South American Climate

J. D. LENTERS AND K. H. COOK

Cornell University, Ithaca, New York

(Manuscript received 18 December 1995, in final form 13 September 1996)

ABSTRACT

The climatological structure in the upper-tropospheric summertime circulation over South America is diagnosed using a GCM (with and without South American topography), a linear model, and observational data. Emphasis is placed on understanding the origin of observed features such as the Bolivian high and the accompanying ''Nordeste low'' to the east. Results from the linear model indicate that these two features are generated in response to precipitation over the Amazon basin, central Andes, and South Atlantic convergence zone, with African precipitation also playing a crucial role in the formation of the Nordeste low. The direct mechanical and sensible heating effects of the Andes are minimal, acting only to induce a weak lee trough in midlatitudes and a shallow monsoonal circulation over the central Andes. In the GCM, the effects of the Andes include a strengthening of the Bolivian high and northward shift of the Nordeste low, primarily through changes in the precipitation field. The position of the Bolivian high is primarily determined by Amazonian precipitation and is little affected by the removal of the Andes. Strong subsidence to the west of the high is found to be important for the maintenance of the high's warm core, while large-scale convective overshooting to the east is responsible for a layer of cold air above the high.

1. Introduction

Upper-tropospheric stationary waves represent some of the most distinct climatological features of the earth's atmosphere. These deviations from the zonal mean are a consequence of inhomogeneities at the surface of the earth (land–sea contrast, orography, etc.) and are observed throughout the globe and over a wide range of length scales. In addition to being a response to forcing at the earth's surface, stationary waves can also be a source of structure for the climate of remote regions through atmospheric teleconnections. For example, the Rocky Mountains and Tibetan Plateau are known to influence Northern Hemisphere storm tracks and dry belts through stationary wave patterns (Broccoli and Manabe 1992).

Of the many types of upper-tropospheric stationary patterns observed in the atmosphere, some of the most well-defined are found in the Tropics and subtropics in the form of closed anticyclones. Figure 1 shows observed streamlines at the 200-mb level for July and January climatologies [from National Aeronautics and Space Administration (NASA) 4D assimilation; see section 2]. During both months, at least four regions of closed anticyclonic circulation are apparent, typically three or four in the summer hemisphere and one in the winter. For July these regions are northwestern Mexico, the Arabian Gulf, the Tibetan highlands, and the western Pacific (around 10°S), while in January the regions of interest are Bolivia, southern Africa, northern Australia, and the western Pacific (near 15°N and 10°S).

Each of these upper-level anticyclones denotes a region of high pressure, accompanied in many cases by a trough to the east. It is generally recognized that upper-level highs such as these are part of a class of thermally induced features that form in regions of high precipitation in response to condensational heating, often representing an upper-level manifestation of the region's summer monsoon (e.g., Hastenrath 1991). A basic theoretical understanding of these tropical features is provided by linear, equatorial models such as those utilized by Matsuno (1966), Webster (1972), and Gill (1980), hereafter referred to as the Gill model. In such models, upper-level high pressure develops as a direct, linear response to imposed midtropospheric heating. The simplicity of such an interpretation is appealing, and the success of the Gill model suggests that it provides a good, first-order understanding.

However, the upper-level tropical anticyclones do not all fit the Gill model interpretation perfectly. The high in the Arabian Gulf, for example, is located a considerable distance from the nearest region of high precipitation. Similarly, it is not likely that the structural dif-

Corresponding author address: Dr. John D. Lenters, University of Wisconsin, Center for Limnology, 680 North Park Street, Madison, WI 53706-1492.
E-mail: jlenters@facstaff.wisc.edu

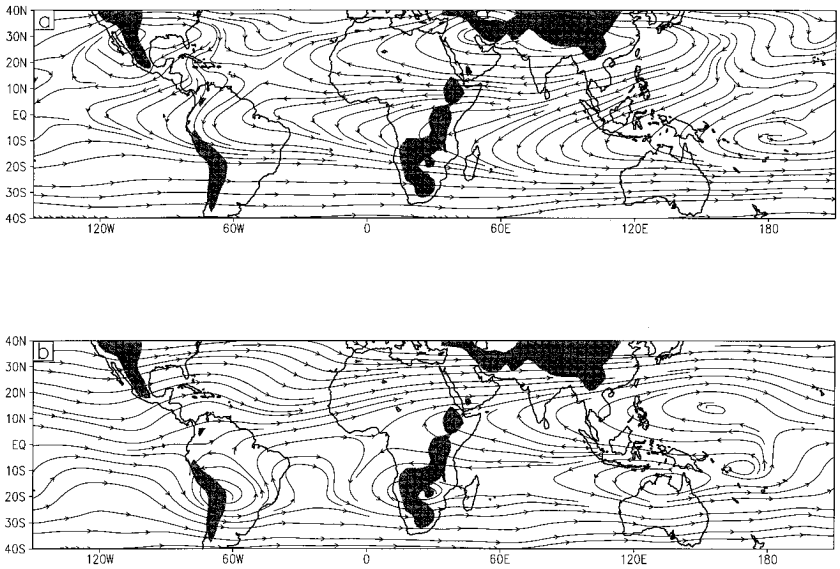

FIG. 1. (a) Climatological streamlines at 200 mb for July (from NASA/DAO 4D assimilation). Shaded regions indicate topography in excess of 1 km. (b) As in (a) but for January.

ferences between the various upper-level highs (Fig. 1) are entirely attributable to variations in precipitation, but that other processes are playing a role as well. Another drawback of simple models such as the Gill model is that the precipitation distribution is assumed a priori, which precludes a truly fundamental understanding of the origin of the precipitation pattern and the upper-level high.

In light of these considerations, it is interesting to note that of the nine high-pressure cells shown in Fig. 1, five are near high topography. This suggests that topography may play a role in the formation of some of these highs, either directly (through sensible heating or obstruction of the flow) or indirectly (e.g., by modifying the precipitation field). Indeed, it is widely accepted that the Tibetan Plateau exerts a significant influence on the Asian summer monsoon and the upper-level Tibetan high (Flohn 1968; Hahn and Manabe 1975; Zheng and Liou 1986). The effects of topography on the upper-level highs of other regions, however, are not as well understood.

In South America, the effect of the Andes on the Bolivian high has received moderate attention yet remains an unresolved issue. Given that the Bolivian high is the dominant feature of the upper-level summertime circulation over South America, a thorough investigation of this feature and its underlying cause is warranted. This study focuses on defining the roles of topography and diabatic heating in generating upper-tropospheric anomalies over South America, with an emphasis on the Bolivian high. This is accomplished by means of a general circulation model (GCM) and linear model, as well as through analyses of the fundamental atmospheric dynamics and thermodynamics of the circulation features and numerous observational comparisons.

The next two sections constitute a review of the Bolivian high and associated circulation features. An observational description of the high's climatological characteristics and its relationship to other circulation features is presented in section 2, while section 3 follows with a comprehensive review of previous observational and modeling studies of the Bolivian high. (The reader who wishes to skip these preliminary sections may begin at section 3c.) These sections identify the unresolved scientific questions and provide a detailed context for the modeling approach used in the current study, which is described in section 4. Model results are presented in section 5, while section 6 provides additional analyses of the climatological balances that characterize the basic physics of the Bolivian high. A summary of the results is given in section 7.

2. Observational description

The climatological data used in this study are taken from the global assimilated dataset produced by the Data Assimilation Office (DAO) at NASA's Goddard Space Flight Center. The dataset represents eight years of observations that have been assimilated using version 1 of the Goddard Earth Observing System atmospheric GCM [see Schubert et al. (1993) for a description of the NASA/DAO assimilation]. An austral summer climatology has been formed by averaging 8 months of January observations (1986–1993). The NASA/DAO data are available on a 2.5° longitude by 2° latitude grid and at 18 pressure levels (or 20 sigma levels). For purposes of comparison with the model results in this study, the data have been interpolated to an R30 transform grid (3.75° longitude by about 2.25° latitude). It should be kept in mind that the assimilated data do not represent

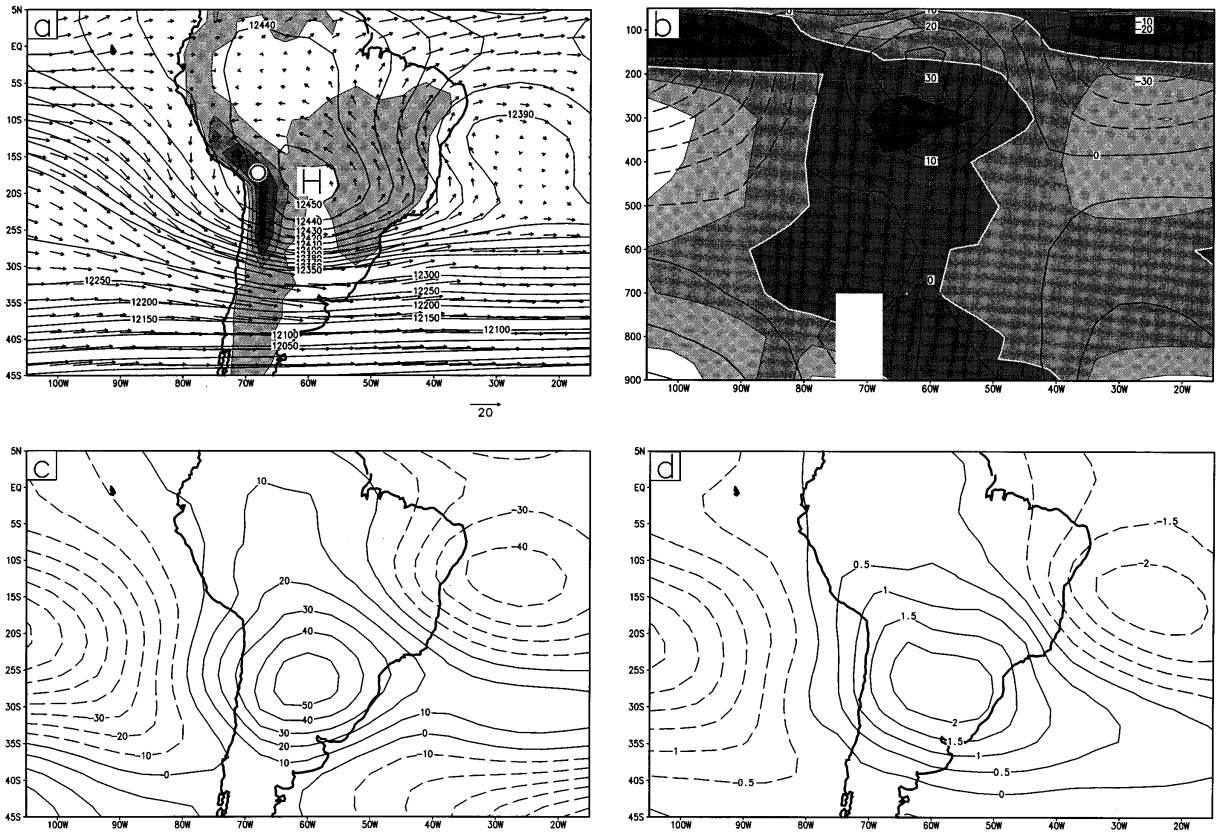

FIG. 2. (a) Geopotential height (maximum denoted by ''H'') and wind vectors at 200 mb from NASA/DAO observations. Above 12 350 m the contour interval is 10 m, while below it is 50 m. Shading denotes topography (contour interval 1000 m, starting at 250 m), and the vector in the lower right corner indicates a wind speed of 20 m s^{-1}. The approximate location of the Altiplano is shown with a white circle. (b) Vertical cross section of eddy geopotential height (contour interval 10 m, negative contours dashed) and eddy temperature (shaded, 1-K interval; white contour denotes the 0-K line and darker shading denotes higher temperature), averaged from 10° to 25°S. (c) Eddy geopotential height at 200 mb (contour interval 10 m, negative values dashed). (d) Eddy temperature at 300 mb (0.5-K contour interval, negative values dashed).

''pure'' observations, but include a certain amount of model bias, especially in data-sparse regions.

At 200 mb, the Bolivian high in the NASA/DAO data is positioned at 19°S and 60°W (Fig. 2a), about 5°–10° to the east of that identified in other observational studies (Kreuels et al. 1975; Virji 1981; Horel et al. 1989). Anticyclonic flow about the high is evident, with winds nearly parallel to the height contours except to the immediate west of the high and north of about 10°S. Easterlies extend to the north of the Bolivian high, with a maximum wind speed of about 6 m s^{-1} occurring at 12°S. Also evident in Fig. 2a (as well as Fig. 1b) is a deep trough to the east of the high, a feature that actually forms a closed low and will be referred to as the ''Nordeste low[1].'' The proximity of the Bolivian high to the elevated plateau of the central Andes (the ''Altiplano,'' see Fig. 2a) is also noteworthy and suggests a possible relationship.

Figure 2b presents a vertical cross section of the Bolivian high, averaged from 10°S to 25°S, along with eddy temperatures (deviations from the zonal mean). As has been noted before (e.g., Kreuels et al. 1975), the Bolivian high is characterized by a warm core below about 150 mb, capped above by a cold top. The warm temperatures extend from the surface and maximize at around 300 mb. Correspondingly, the eddy geopotential height is positive above 500 mb, with a maximum between 150 and 200 mb. The Nordeste low to the east has opposite characteristics, with a cold core and warm top.

As shown in Figs. 2c and 2d, the eddy geopotential height and temperature fields depict the extensive horizontal scale of the Bolivian high. Anomalously high pressure (Fig. 2c) and temperature (Fig. 2d) between about 80°W and 50°W extend from north of the equator down to about 40°S, reaching maximum values 5°–10° south of the full-field high (the ''H'' in Fig. 2a). The high geopotentials (and temperatures) even extend to the east-southeast over the Atlantic Ocean around 30°S.

[1] The closed low is in relatively close proximity to the northeastern tip of Brazil, a region known as the ''Nordeste.''

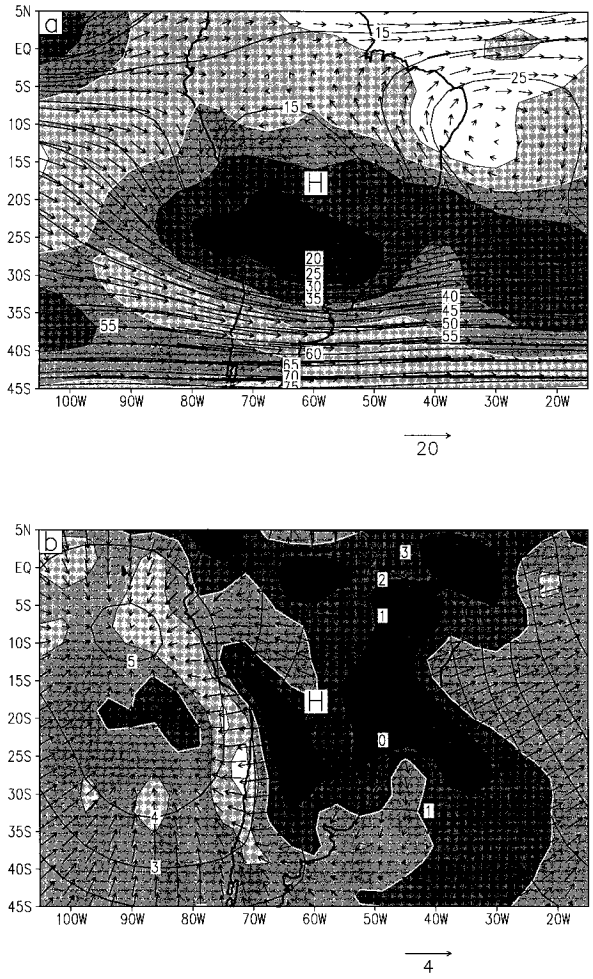

FIG. 3. (a) Observed 200-mb streamfunction (contour interval 5×10^6 m^2 s^{-1}) and nondivergent wind vectors (20 m s^{-1} shown in the lower right corner). Shading indicates relative vorticity (contour interval 1×10^{-5} s^{-1}), with the zero line shown in white and darker shading indicating higher relative vorticity. Here, ''H'' gives the location of the Bolivian high. (b) Observed velocity potential (contour interval 1×10^6 m^2 s^{-1}) and divergent wind vectors (4 m s^{-1} shown in the lower right corner). Shading indicates horizontal wind divergence (contour interval 2×10^{-6} s^{-1}), with the zero line shown in white and darker shading indicating stronger divergence.

The Nordeste low and its cold core are also clearly shown in the eddy fields.

Figure 3a shows the streamfunction, relative vorticity, and nondivergent winds at 200 mb. While there is good correspondence between the streamfunction (Fig. 3a) and geopotential height (Fig. 2a), the streamfunction minimum is located about 5° west of the Bolivian high. This may either be a real feature or a reflection of the difficulty in observing geopotential height in the Tropics. A band of maximum relative vorticity stretches from east to west about 5°–10° south of the Bolivian high, attaining a maximum value of 3×10^{-5} s^{-1} at 25°S, 60°W. This is in reasonably good agreement with the observations of Virji (1981).

Figure 3b characterizes the divergent component of the circulation. Note that the maximum geopotential represents neither a center of divergent outflow (as represented by the velocity potential) nor a region of maximum horizontal wind divergence. Instead, the large-scale center of outflow is located 10°–15° to the east. Regions of maximum divergence are located throughout the region, the strongest being to the east of the high along 45°W and to the immediate southwest (23°S, 64°W). Strong upper-level convergence occurs about 15° to the southwest of the high.

The features of the divergent circulation (Fig. 3b) do not agree as well with the results of Virji (1981) as do those of the rotational component. For example, in Virji (1981) the divergent center is located at about 7°S and 63°W, and divergent winds exceed speeds of 10 m s^{-1} in places. In Fig. 3b, wind speeds are no larger than 3 m s^{-1} and in most regions represent no more than 20% of the total wind speed. This disagreement is probably due to the different periods of observation and the difficulty in accurately observing the divergent component of the circulation. (In the case of the NASA/DAO data, the divergent component is also sensitive to the assimilation model's simulated precipitation field.) However, we have also consulted January analyses from European Centre for Medium-Range Weather Forecasts (ECMWF) (1980–1989) and found them to be in better agreement with Fig. 3b than the results of Virji (1981). In particular, the ECMWF data show a divergent center at 12°S, 55°W and divergent wind speeds of less than 3 m s^{-1}.

3. Current understanding of the Bolivian high

a. Climatic significance

The Bolivian high is intimately related to other features of the South American climate. Numerous observational studies have noted a relationship between the seasonal variation in South American rainfall and the position and intensity of the Bolivian high (Kousky and Kagano 1981; Nishizawa and Tanaka 1983; Horel et al. 1989). It is also recognized that the Bolivian high and the Nordeste low are dynamically linked (Kreuels et al. 1975; Horel et al. 1989) and that the low is associated with sinking motion (Virji 1981) and the dry climate of northeast Brazil (Nishizawa and Tanaka 1983). Furthermore, the Bolivian high and Nordeste low may be related to convection and cold frontal penetrations associated with the South Atlantic convergence zone (SACZ; Kousky and Kagano 1981; Kodama 1992, 1993). The position of the Bolivian high has also been related to the interannual variability of precipitation on the Bolivian–Peruvian Altiplano (Kessler 1981; Lenters 1997).

The relevance of the Bolivian high is not limited to the time-mean climate, as the high can often be resolved on shorter timescales, even individual days (Virji 1981).

As a feature of South American weather, it exhibits significant variations in position and intensity (Virji 1981). This short-term variability has been related to other aspects of the synoptic meteorology of South America. For instance, propagating upper-tropospheric cyclonic vortices in the region of the Nordeste low interact with the Bolivian high and modulate convection in the region (Kousky and Gan 1981; Virji 1981). Aceituno and Montecinos (1993) and Lenters (1997) have also noted a relationship between the Bolivian high and the episodic nature of summer precipitation on the Altiplano; during wet days the Bolivian high is more intense and displaced farther south than during dry days.

b. Fundamental cause: Andean topography or Amazonian heating?

To the authors' knowledge, Schwerdtfeger (1961) was the first to acknowledge the existence of the Bolivian high over the subtropical highlands of the Andes. He found that the anticyclone is absent in winter and concluded that the dynamic effect of the Andes is not important in generating the upper-level high. Instead, Schwerdtfeger (1961) hypothesized that the feature is thermally induced by condensational heating over the Altiplano, itself a source of sensible heat.

Using conventional meteorological data, Gutman and Schwerdtfeger (1965) performed an analysis of the atmospheric heat budget over the Altiplano region. Latent heat released in thunderstorms over the plateau was determined to be the primary heat source for the Bolivian high, with sensible heating contributing less than half as much heat. Some of this heating was balanced by cold air advection from the west, and it was noted that the Bolivian high is capped by a cold layer above 175 mb, as a result of ''high reaching convective activity'' (Gutman and Schwerdtfeger 1965). The general conclusion offered by Gutman and Schwerdtfeger (1965) is that the intense sensible heating of the atmosphere over the Altiplano drives the convergence of moisture-laden winds, latent heat release in thunderstorms, and the formation of the Bolivian high.

The work of Gutman and Schwerdtfeger (1965) regarding the cause of the Bolivian high remained the prevailing wisdom for nearly two decades (Kreuels et al. 1975; Virji 1981). But it was pointed out by Silva Dias et al. (1983) that the Bolivian high might be the result of latent heat released over the Amazon basin (as opposed to the Altiplano). To test this hypothesis, Silva Dias et al. (1983) employed a time-dependent Gill-type model (with one vertical mode) forced by idealized transient heating at the approximate latitude of the Amazon basin. A unique feature of the study was the partitioning of the response into Kelvin, Rossby, gravity, and mixed Rossby–gravity modes. The imposed heating was turned on at time $t = 0$ h, reached a maximum at $t = 12$ h, and became negligible by $t = 48$ h. In response, an upper-level high-pressure cell developed directly above the region of maximum forcing. By $t = 32$ h the high pressure had split into two distinct features, an eastward propagating Kelvin wave (northeast of the heating maximum) and a westward propagating Rossby wave (southwest of the heating maximum). The Rossby wave response, a well-defined anticyclone, bore a close resemblance to the Bolivian high. Especially striking was the ability of this model to explain how the Bolivian high, as a southwestward propagating Rossby wave, could be positioned over the Altiplano even though the forcing was over the Amazon basin. However, since topography was not incorporated in the model, the effects of the Andes on the Bolivian high remained uncertain.

The work of Silva Dias et al. (1983) was extended by DeMaria (1985), who used the same linear model, but with 13 vertical modes, to study the steady and transient responses to Amazonian heating. The transient response agreed with the results of Silva Dias et al. (1983) except away from the forcing, where some vertical propagation of energy was evident. For the steady-state case, the climatological Bolivian high was well simulated, again positioned southwest of the heating maximum. The cold core Nordeste low was not simulated in the steady-state case, but a weak trough developed in the transient response. The poor simulation of this feature suggested to DeMaria (1985) that it is ''not a direct linear response to convective forcing'' and that nonlinear effects are important. As in Silva Dias et al. (1983), the role of the Altiplano was not discussed.

Interest in the thermal influence of the Altiplano was revived with the work of Rao and van de Boogaard (1986) and Rao and Erdogan (1989). An estimate of the heat budget over the Altiplano was performed by Rao and Erdogan (1989) in a manner similar to that of Gutman and Schwerdtfeger (1965) but with a larger number of surface stations and additional satellite data. They concluded that net heating of the atmosphere occurs over most of the Altiplano, with sensible heating dominating in the western portions of the Altiplano and condensational heating prevailing in the eastern portions. Although Rao and Erdogan (1989) presented convincing evidence of a heat source over the Altiplano, the effects on the Bolivian high were not explicitly investigated, and the significance of Amazonian heating was not discussed.

Beginning with Kleeman (1989), modeling studies of the Bolivian high began to incorporate the effect of the Andes. Similar to Silva Dias et al. (1983) and DeMaria (1985), Kleeman (1989) used a linear equatorial β-plane model to investigate the effects of a transient Amazonian heat source on the circulation over South America. The Andes were included as a meridional (''knife edge'') barrier in the lowest layer of the two-level model. While the effect of the barrier on the low-level circulation was pronounced, the upper-level circulation was qualitatively very similar to that of Silva Dias et al. (1983) and DeMaria (1985). The only effect on the Bolivian high

was a westward extension of the high pressure and a slight weakening of the northerly winds on the western edge of the high. There was also some evidence that the trough to the east of the Bolivian high was strengthened.

Gandu and Geisler (1991) turned to a nonlinear, primitive equations model with five sigma levels in the vertical. The steady and transient responses to Amazonian heating were investigated with and without idealized Andean topography. Again, the mechanical influence of the Andes on the Bolivian high was minimal. Gandu and Geisler (1991) also concluded that the effects of nonlinearity, in both the steady and transient cases, were not significant. However, it was found that nonlinearities as well as the inclusion of a basic-state zonal flow helped to define the trough east of the Bolivian high (though this feature was still only weakly simulated).

More recently, Figueroa et al. (1995) investigated the effects of a diurnally varying Amazonian heat source on the summer circulation using an eta coordinate model. The model solves the primitive equations on seven vertical levels, with the Andes included in the form of step topography. The simulation of the upper-level circulation was much the same as in the previous studies, with a strong Bolivian high to the southwest of the heat source and a weak trough to the east. Neither of these features was significantly affected by the obstruction of the flow by the Andes. One new result was the simulation of low-level wind convergence in the region of the SACZ in response to Amazonian heating. This transient feature was most intense 18 hours after the time of maximum heating and could not be effectively simulated with a steady heat source.

c. Summary: What questions remain?

The studies reviewed above have convincingly shown that the Bolivian high can be understood as a Rossby wave response to condensational heating over the Amazon basin. The climatological positioning of the high over the Altiplano, 10°–15° southwest of the region of maximum heating, can be explained by the southwestward propagation and subsequent decay of this Rossby wave during repeated episodes of convection. The direct, mechanical effect of the Andes on the Bolivian high (i.e., through obstruction of the flow) is minimal.

Despite this understanding, many questions remain unanswered. One issue involves a complete treatment of the role of the Andes. The direct mechanical effects have been shown to be small, but only in the framework of purely dynamical models with no feedback between the flow field and the diabatic heating field. Given the potential influence of the Andes on the precipitation field, especially in the Amazon region, *indirect* effects of the Andes on the Bolivian high could be significant. Furthermore, while the Altiplano has been shown to be a net source of heat for the atmosphere, no attempt has been made to explicitly model its effects on the Bolivian high.

Another outstanding issue is the influence on the Bolivian high of precipitation in regions other than the Amazon. The summer precipitation field over South America shows a considerable amount of structure and hardly fits the idealization of a single maximum over the Amazon basin (Lenters and Cook 1995). Condensational heating in the central Andes (including the Altiplano) and the SACZ, for example, could be important for the maintenance of the Bolivian high and deserves investigation.

The Bolivian high has been mainly investigated within the framework of linear dynamics. Nonlinearities, while not fundamental to the generation of the Bolivian high, have not been explored in detail and may play a more significant role than has been previously indicated. Furthermore, the cold layer capping the Bolivian high has received minimal attention and still lacks a complete explanation.

Finally, the geographically extensive nature of the Bolivian high (such as its southeastward extension over the South Atlantic) remains a poorly understood issue, as does the origin of the Nordeste low. The previous studies have indicated that the Nordeste low is not simulated as part of a steady, linear response to Amazonian heating. A weak trough is present in the transient simulations, and it has been noted that topography, nonlinearity, and a basic-state flow help to define this trough. Nevertheless, a well-defined closed vortex in the vicinity of the Nordeste low is absent from all of the previous studies, indicating the need for further research.

4. Description of models and experimental design

a. GCM

To investigate the issues raised above, the summertime circulation over South America is analyzed using a GCM and linear model. The GCM is a version of the model developed and maintained at National Oceanic and Atmospheric Administration (NOAA) Geophysical Fluid Dynamics Laboratory (GFDL). It is a global, atmosphere-only, spectral model and solves the primitive equations in sigma coordinates, along with a prognostic equation for water vapor mixing ratio [see Manabe (1969) for a description of the model]. The horizontal resolution used in this study is R30, which corresponds to 3.75° longitude by about 2.25° latitude on the transform grid. In the vertical, 30 sigma levels are employed, with closest spacing occurring near the surface and the tropopause.

The model time step is 16 min, and moist convective adjustment is used to parameterize cumulus convection. Solar insolation does not vary diurnally or seasonally, but is fixed at the austral summer solstice (''perpetual January''). Clouds are fixed in a zonally uniform, hemispherically symmetric distribution using observed, an-

nual mean, Southern Hemisphere values. Ozone concentrations are also zonally uniform and the same in both hemispheres. The GCM is spun up from an isothermal atmosphere at rest, and the first 300 days are discarded. The remaining 2200 days are averaged to form a climatology.

In order to isolate the fundamental surface–atmosphere interactions that lead to the generation of the Bolivian high, many of the surface conditions in the GCM have been specified in an idealized manner. The exceptions are topography and sea surface temperatures (SSTs), which have realistic distributions. The January SSTs are those of Shea et al. (1990). The topography has been filtered (A. J. Broccoli, 1993, personal communication) to reduce Gibbs ripples that are especially strong near the steep and narrow Andean topography. This significantly improves the simulation of precipitation in the vicinity of the Andes. However, the maximum height of the Andes is significantly reduced, reaching only about 2 km, as opposed to the observed height of 3.8 km.

Land surface albedo is specified to be 0.11 everywhere except over glaciated land and snow-covered regions, where the albedo is calculated. Ocean albedo is 0.08 except in areas of sea ice, where higher values are prescribed. Soil moisture is fixed at 10 cm over land and 15 cm (saturation) over ocean. The surface drag coefficient is a factor of 3 larger over land than over ocean except in glaciated regions, where it is identical to the ocean value.

These land surface parameters were chosen for various reasons. An accurate simulation of the Bolivian high depends largely on the ability of the model to reasonably simulate the summertime precipitation distribution over South America (particularly in the Amazon basin), and this does not require geographic structure in the GCM's land surface conditions [other than topography, see Lenters and Cook (1995)]. In addition, these experiments are designed to investigate the physical basis for the generation of the Bolivian high, including a clean mountain/no-mountain comparison. But much of the structure in the surface moisture and albedo distributions is associated with topography, so it does not seem appropriate to include such structure in the no-mountain case. For these reasons geographically uniform land surface parameters are chosen, using values which approximate conditions over the Amazon basin. However, the accuracy of the heating rates over the Altiplano, where the land surface is drier and of higher reflectivity than in the Amazon, may be compromised; this concern is addressed in the next section.

Two GCM experiments are performed in this study and are referred to as the ''control'' and ''no-Andes'' experiments. The control experiment has the boundary conditions detailed above. The no-Andes experiment is identical to the control, except that all South American topography has been removed. This provides a clean diagnosis of the net influence of the Andes on the Bolivian high, including indirect effects such as changes in the precipitation field.

b. Linear model

To separate the individual effects of topography and diabatic heating, a linear model is employed. The model is that described by Ting and Held (1990) and is a steady-state, linearized version of the GCM's dry dynamics. The primitive equations are linearized about a zonally uniform basic state and forced by topography, diabatic heating, and transient eddies (terms involving the product of deviations from the time mean). Solution of the equations is performed through matrix inversion. Both the basic-state fields and the forcing functions are taken from the GCM control experiment. The transient forcings are calculated explicitly during the course of the GCM integration, except for the vorticity transients, which are calculated as a residual. With good agreement between the GCM climatology and the full linear model solution (i.e., with all the forcings included), the linear model can be used to diagnose the effects of individual forcings.

Dissipation in the linear model takes the form of Rayleigh friction and Newtonian cooling, as well as biharmonic diffusion ($\nu\nabla^4$; $\nu = 10^{17}$ m^4 s^{-1}) of vorticity, divergence, and temperature. The coefficient of biharmonic diffusion is 10 times greater than in the GCM and provides a smoother response (Ting and Held 1990). Rayleigh friction and Newtonian cooling are included primarily to account for low-level dissipative and nonlinear effects, but some weak damping is also included in the free atmosphere. The thermal and mechanical damping rates are both (25 days)$^{-1}$ in the free atmosphere ($\sigma = 0$ to 0.8), increasing linearly to a value of (5 days)$^{-1}$ at the surface ($\sigma = 1$). For Newtonian cooling, an additional approximation to damp on pressure levels instead of sigma is included, a difference that can be significant over topography. The choice of damping rates is based on the work of others (DeMaria 1985; Valdes and Hoskins 1989; Gandu and Geisler 1991), as well as some sensitivity studies of our own, which indicate that the simulation of the Bolivian high is not particularly sensitive to the choice of damping rates.

Many linear model experiments have been performed to isolate the sources of structure in the upper-level circulation field. Individual forcings include diabatic heating (broken down into radiative, condensational, and sensible heating[2]), transient eddies (broken down into vorticity, divergence, and thermal transients), and me-

[2] The forcing for sensible heating includes the GCM's dry convective heating field (parameterized as dry adiabatic adjustment) as well as the turbulent flux of sensible heat. These two forcings have been combined, because their individual contributions to the vertical heat flux are intimately related and significant cancellation often occurs at low levels.

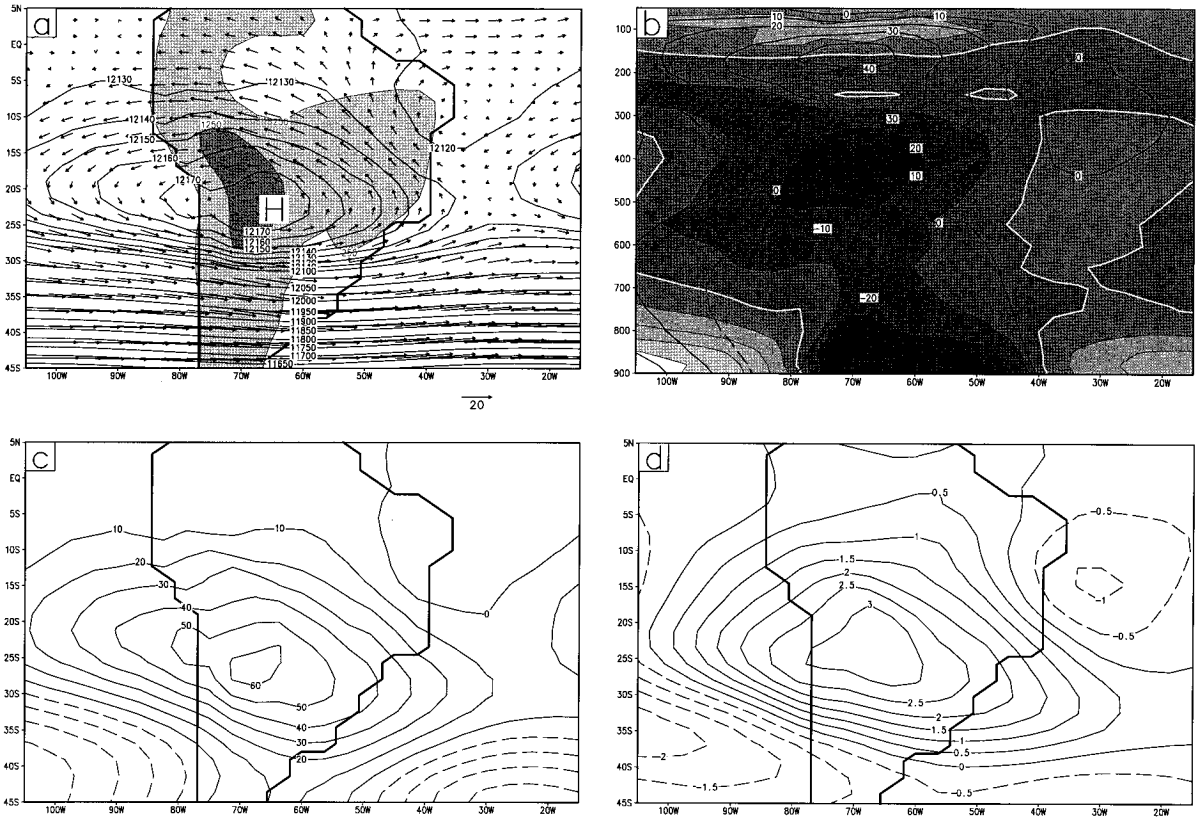

FIG. 4. As in Fig. 2 but for the control GCM experiment. The contour interval in (a) is 10 m above 12 100 m and 50 m below. Temperatures in (d) are shown at 400 mb.

chanical forcing by topography. In addition, some of the forcing fields are divided up geographically, in order to determine responses to regional forcing. In particular, this allows individual consideration of the influence of mechanical forcing by the Andes, sensible heating over the Altiplano, and condensational heating over the Amazon, central Andes, and SACZ. Although the total number of linear model experiments is rather large, only those that contribute significantly to the total response are discussed.

5. Model results

a. GCM control simulation: Comparison with observations

To evaluate the GCM's control simulation of the Bolivian high, we compare observed and modeled fields of geopotential height, temperature, and wind velocity in the South American region. The modeled maximum geopotential height at 200 mb (Fig. 4a) is located at about 24°S and 64°W, which is just to the southwest of the observed position of the Bolivian high (Fig. 2a). The modeled and observed winds and geopotential gradient to the south and east of the high also compare favorably. The GCM, however, simulates an elongated Bolivian high, stretching the high pressure and associated circulation to the west (Figs. 2a and 4a). In addition, the tropical easterlies to the north of the high are stronger in the GCM (by up to 10 m s^{-1}) and extend farther to the west. The Nordeste low is modeled to the east of the Bolivian high, as evidenced by the cyclonic circulation in Fig. 4a. However, the low is located 5°–10° northwest of its observed position. This equatorward positioning acts to further distinguish the closed cyclonic circulation from the remainder of the trough to the south while at the same time weakening the corresponding geopotential height anomaly.

The GCM captures most features of the Bolivian high's vertical structure (Fig. 4b). However, the modeled warm core has its maximum eddy temperature at 400 mb, while the observations show a maximum at 300 mb. (This may be due to the shallow nature of the model's moist convective adjustment.) Also evident in Fig. 4b is the model's unrealistic westward extension of the Bolivian high and generally weak geopotential gradient to the west. The cold core of the Nordeste low is captured in the model, but not as strongly as in the observations.

Modeled height and temperature anomalies associated

with the Bolivian high are shown in Figs. 4c and 4d.[3] Again, the unrealistic westward elongation of the Bolivian high is pronounced. However, the southeastward extension of the high and its warm core is correctly captured. The cold core of the Nordeste low also shows up clearly in the model temperature field, but the low is not as well defined in the eddy geopotential field.

Despite some notable differences between the observations and the results of the control experiment, the position and intensity of the Bolivian high are reasonably well simulated by the GCM, as is the associated warm core, its extension to the east-southeast, and the cold-core Nordeste low. This suggests that the model is reasonably representative of the real climate and is capable of addressing questions related to the origin of these features.

It is also worthwhile to compare the diabatic heating rates in the GCM with observed rates since these forcings are utilized in the linear model experiments. One should keep in mind, however, that the weight given to such a comparison is limited by the large uncertainty in observed diabatic heating rates. Figures 5a and 5b show the sensible heat flux in the control experiment and NASA/DAO assimilated data, respectively. Near the Altiplano the model simulates sensible heat fluxes of about 35 W m^{-2}, roughly half that found in the NASA/DAO data. The results of Rao and Erdogan (1989) suggest that the discrepancy may be even greater, as their estimates of sensible heating in the central Andes exceed 125 W m^{-2}. We have run additional GCM experiments to examine the reasons for the GCM's weak sensible heat flux over the Altiplano. Although not the focus of this study, it is worth noting that (in the GCM) higher topography and, especially, realistic albedo and soil moisture increase the sensible heat flux in the central Andes region. The greatest effect is south of the Altiplano, between 20°S and 35°S, where heating rates are increased by at least 50%.

Figures 5c and 5d show vertically integrated condensational heating rates in the control experiment and NASA/DAO observations, respectively. Modeled heating rates tend to be higher than the observed, especially in the Amazon and central Andes, but the overall structure is well simulated. Modeled and observed heating maxima are also present in the northern and southern Andes as well as in the SACZ. These maxima have also been identified in the precipitation dataset of Legates and Willmott [1990; see Lenters and Cook (1995)], which shows vertically integrated heating rates in excess of 300 W m^{-2} in the Amazon and central Andes. Rao and Erdogan (1989) have even measured heating rates of over 500 W m^{-2} in a small region immediately to the east of the Altiplano for the month of January 1979. Thus, the condensational heating rates modeled in the GCM may not be as excessive as a comparison of Figs. 5c and 5d suggests.

b. Linear model diagnosis: Effects of individual forcings

Before breaking down the linear model response, we must first validate the linear solution by comparing the results with those of the GCM control experiment. Figure 6 shows geopotential height, wind velocity, and temperature from the linear model with all forcings included except topography.[4] At 200 mb the linear model simulation of the Bolivian high and Nordeste low (Fig. 6a) compares well with that of the GCM control experiment (Fig. 4a). The high is not as zonally elongated as in the GCM and the Nordeste low is positioned farther south. In these respects, the linear model actually agrees better with the observations (Fig. 2a) than does the GCM. The vertical structure of the linear model response (Fig. 6b) is very similar to that of the control experiment (Fig. 4b), with the Bolivian high and Nordeste low simulated above warm and cold cores, respectively. However, the Bolivian high is notably shallower, maximizing around 350 mb as opposed to 150–200 mb in the GCM. Similarly, the warm core is strongest around 500 mb (Fig. 6b) instead of 400 mb as in the GCM (Fig. 4b). Nevertheless, at these levels the horizontal structure of the Bolivian high (Fig. 6c) and its warm core (Fig. 6d) compares well with the GCM (Figs. 4c and 4d), including the southeastward extension over the Atlantic Ocean.

The linear model's shallow simulation of the Bolivian high may be due in part to the GCM's condensational heating profile, as previous linear model studies of the Bolivian high (which imposed significantly deeper convective heating) have not shown a similar deficiency. On the other hand, the fact that the GCM correctly simulates the Bolivian high at 150–200 mb is an indication that nonlinearities play an important role in raising the height of the response. In support of this notion, Gill and Phlips (1986) note that the level of maximum vertical velocity is displaced above the level of maximum heating when nonlinearities are considered.

To investigate the linear model response to various forcings, upper-level fields of eddy streamfunction are compared (Fig. 7). The fields are left on sigma surfaces in order to ensure that the linear solutions remain exactly additive and to avoid interpolation errors over topography. Given the shallow nature of the linear model response, as noted above, solutions are presented at the $\sigma = 0.34$ level. The full linear model response (Fig. 7a)

[3] Eddy temperatures are shown at 400 mb (instead of 300 mb as in Fig. 2d) because this is the level where the model's warm core reaches a maximum.

[4] Topographic forcing is left out to avoid significant sigma-to-pressure interpolation errors over the Andes. As will be seen, the effects of topography are of second order and do not significantly change the full linear model solution.

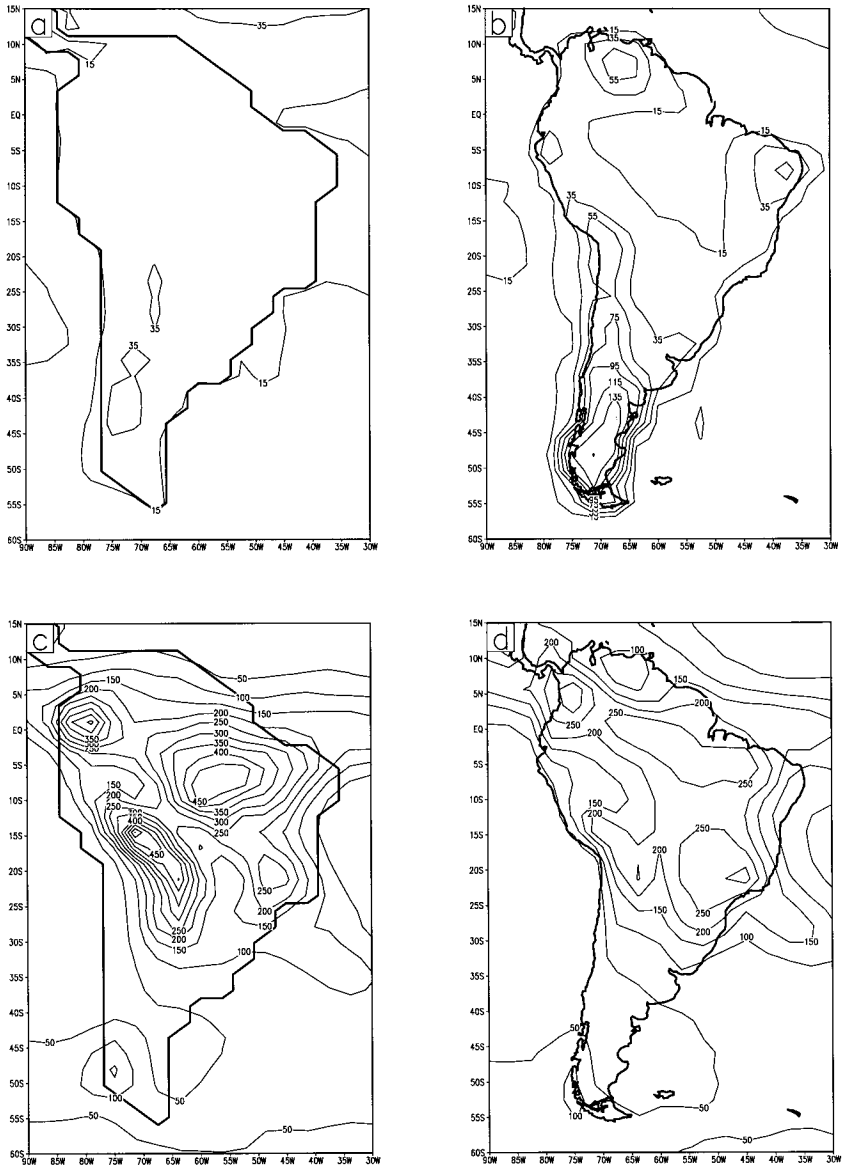

FIG. 5. Sensible heating rates from (a) the control experiment and (b) NASA/DAO observations. Contour interval is 20 W m^{-2}, starting at 15 W m^{-2}. (c) and (d) As in (a) and (b), respectively, but for vertically integrated condensational heating rates (contour interval 50 W m^{-2}).

shows a number of distinct circulation features, including the Bolivian high, Nordeste low, and an extratropical trough over the South Atlantic. The southeastward extension of the high is also evident in Fig. 7a.

In breaking down the full response into its individual components, it is found that the three circulation features identified in Fig. 7a are largely a response to three forcing terms, condensational heating (Fig. 7b), forcing by the thermal transients (Fig. 7c), and mechanical forcing by topography (Fig. 7d). The remaining terms (vorticity and divergence transients, radiative and sensible heating) generate negligible structure in the upper-level circulation field. By far, the dominant forcing is that of condensational heating (Fig. 7b), which is responsible for generating a strong Bolivian high (including its extension to the southeast) as well as the Nordeste low.

While many other modeling studies have also simulated the Bolivian high in response to prescribed midtropospheric heating (Silva Dias et al. 1983; DeMaria 1985; Kleeman 1989; Gandu and Geisler 1991; Figueroa et al. 1995), the southeastward extension of the high and a distinct Nordeste low were not successfully modeled in those studies, which only considered heating over the Amazon basin. This suggests that condensational heating elsewhere is responsible for generating these features. To test this hypothesis, the condensa-

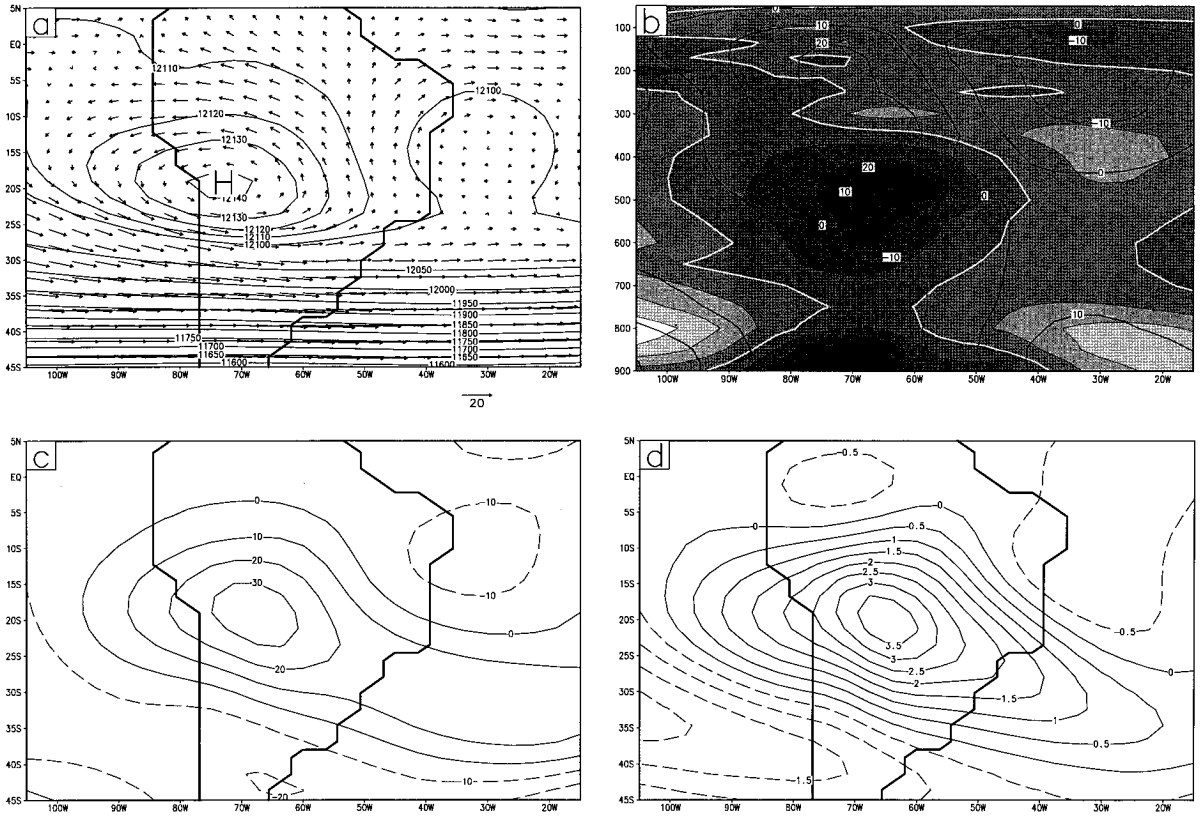

FIG. 6. As in Fig. 2 but for the linear model with full forcing (minus topography). The contour interval in (a) is 10 m above 12 100 m and 50 m below. Geopotential heights in (c) are shown at 350 mb, and temperatures in (d) are at 500 mb.

tional heating response has been broken down into three regions, namely the Amazon (Fig. 7e), central Andes (Fig. 7f), and SACZ (Fig. 7g), with the sum of the three shown in Fig. 7h.

Each region exhibits a Gill-like response, with high pressure (low streamfunction) located to the southwest of the precipitation maximum (Fig. 5c). The response to Amazonian heating (Fig. 7e) is very similar to the steady-state results of DeMaria (1985) and Gandu and Geisler (1991) and is clearly responsible for a large portion of the Bolivian high's structure (Fig. 7b). Heating over the central Andes intensifies southwestern portions of the high (Fig. 7f), while the SACZ is responsible for the southeastward extension of the anomaly over the South Atlantic (Fig. 7g). The total condensational heating rate in the Amazon region (integrated over the area shown in Fig. 7e) is more than 50% higher than that in the central Andes or SACZ, yet the responses to these three forcings are comparable in magnitude (Figs. 7e–g). This tendency for a stronger Rossby wave response in higher latitudes, given the same forcing, has been noted before (e.g., Silva Dias et al. 1983) and is related to stronger vortex stretching (Phlips and Gill 1987).

A comparison of Figs. 7b and 7h reveals that while South American precipitation accounts for most of the structure in the Bolivian high, condensational heating elsewhere does strengthen (weaken) the circulation to the west (north and east) of the high. In addition, one circulation feature that is conspicuously missing in Fig. 7h (but is present in Fig. 7b) is the Nordeste low. The cyclonic circulation surrounding the northern, western, and southern boundaries of the Nordeste low (Fig. 7b) is clearly associated with condensational heating over South America (Fig. 7h), primarily that of the Amazon (Fig. 7e) and SACZ (Fig. 7g). But the northerly flow along the eastern boundary of the Nordeste low is not simulated as a response to South American condensational heating (Fig. 7h). Further regional analyses using the linear model have revealed that it is predominately African precipitation, in association with the upper-level African high, that closes off the circulation in Fig. 7h to form the Nordeste low (Fig. 7b).

The upper-level response to the thermal transients (Fig. 7c) is roughly one-third the response to condensational heating and of opposite sign. Thus, the effect at this level is to partially offset the effects of latent heating (Fig. 7b), thereby weakening the total response (Fig. 7a). Ting and Held (1990) also found significant compensation between tropical anomalies forced by diabatic heating and by transient eddies. It was not indicated in that study whether the vorticity or thermal tran-

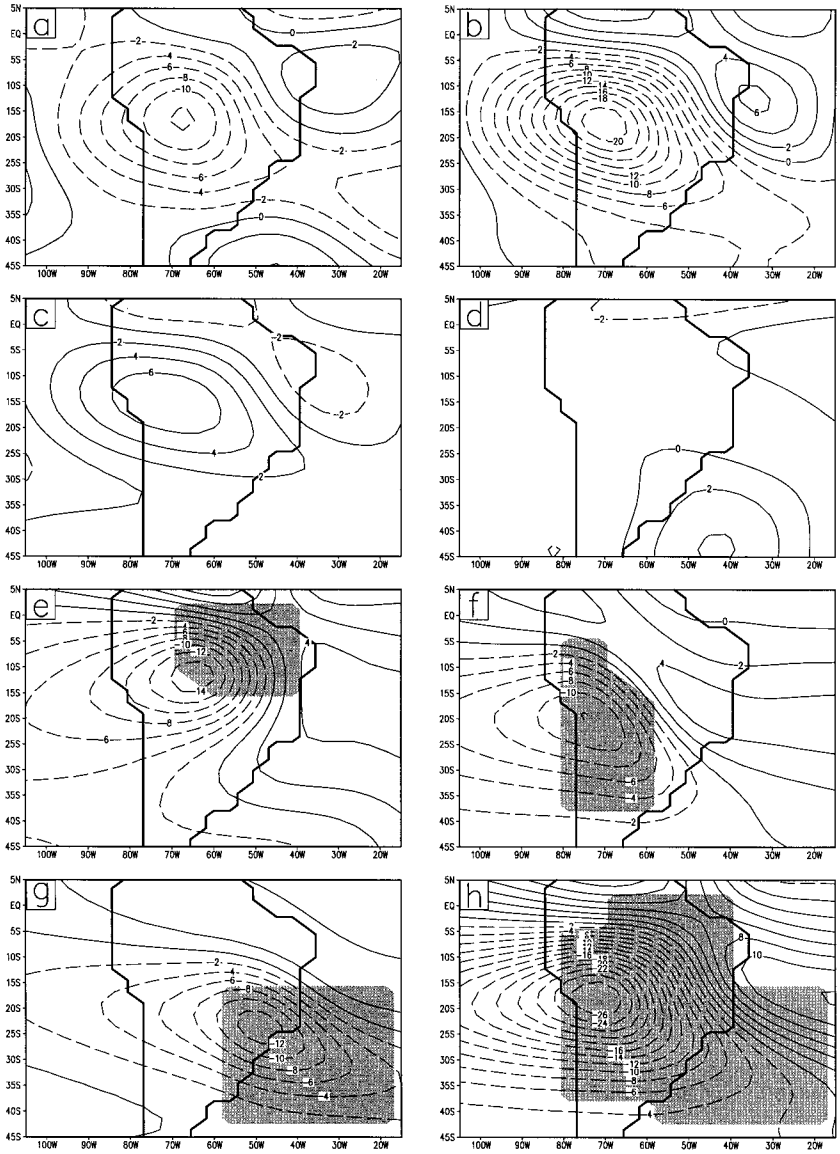

FIG. 7. Eddy streamfunction at $\sigma = 0.34$ from the linear model with (a) full forcing, (b) condensational heating, (c) thermal transient forcing, (d) mechanical forcing by topography, and condensational heating restricted to (e) the Amazon basin, (f) the central Andes, (g) the SACZ, and (h) all three regions. Contour interval is 2×10^6 m^2 s^{-1}, and shading in (e)–(h) indicates the geographic extent of the imposed forcing.

sients were responsible for offsetting the tropical anomalies, but the results of the present study seem to suggest the latter. At this point it should be cautioned that the thermal transients show a significant amount of vertical structure, and that to interpret their effects as a simple damping of the diabatic heating response is an oversimplification. In section 6 we present a more in-depth analysis of the thermal transients and offer a reinterpretation of their role.

The primary effect of topography on the upper-level circulation (Fig. 7d) is to induce an extratropical trough in the lee of the Andes. Though this trough is relatively weak, it is present in the full linear model simulation (Fig. 7a), as well as the GCM control experiment (Fig. 4c) and NASA/DAO observations (Fig. 2c). A regional breakdown of the topographic response reveals that the trough is solely due to the Andes, not to the topography of remote regions. Previous studies have also argued for the presence of a lee trough to the east of the Andes (Boffi 1949; Satyamurty et al. 1980), but its small amplitude has made it notoriously difficult to depict in the observations (Vergeiner and Ogura 1972; Rooney and Janowitz 1979). As has also been noted before (e.g., Gandu and Geisler 1991), the direct, mechanical effects

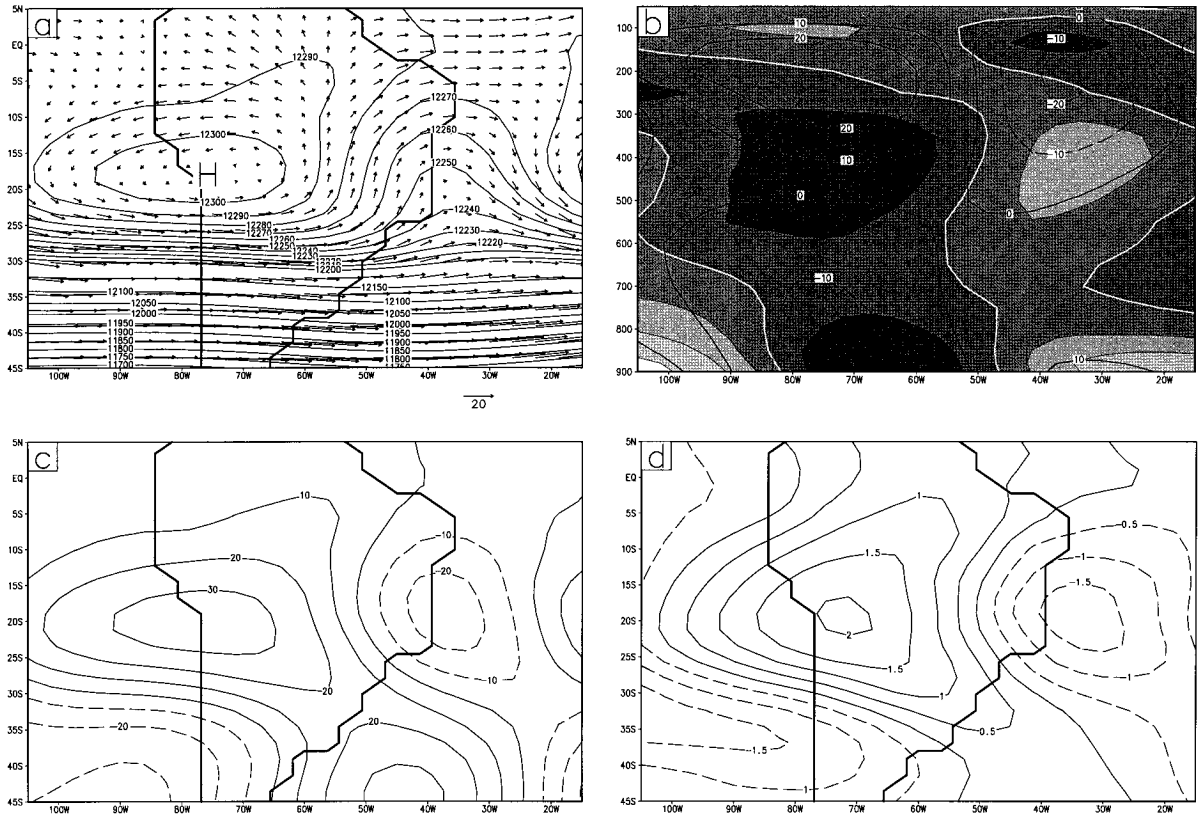

FIG. 8. As in Fig. 2 but for the no-Andes experiment. The contour interval in (a) is 10 m above 12 200 m and 50 m below. Temperatures in (d) are shown at 400 mb.

of topography on the Bolivian high are insignificant (Fig. 7d).

The linear model's negligible upper-level response to sensible heating, being dependent on the GCM's unrealistically low topography and sensible heating rates (Figs. 4a and 5a), deserves comment. The vertical structure of the linear model response to sensible heating over the Altiplano reveals low pressure at the surface topped by high pressure at $\sigma = 0.9$. This weak monsoonal circulation system becomes negligible by $\sigma = 0.7$ and is analogous to a shallow Bolivian high, including a warm core and cold cap. The linear response to stronger forcing (with the same vertical scale) would be greater in magnitude but not in vertical extent. Even in the presence of a realistically elevated Altiplano (surface pressure $\approx$ 650 mb), no significant linear response would occur above 450 mb. Thus, it is concluded that sensible heating does not directly force the Bolivian high, at least in the linear framework. However, this framework does not account for indirect effects such as the influence of sensible heating or mechanical topographic forcing on central Andean condensational heating; forcing that has been shown to significantly affect the Bolivian high. Such nonlinear effects are explored with the no-Andes GCM experiment.

c. *Net effect of topography: The no-Andes experiment*

Figure 8 shows the 200-mb geopotential height, wind velocity, and temperature from the no-Andes GCM experiment. Quite clearly, the Bolivian high is generated in the model even in the absence of South American topography. The high (Fig. 8a) is located 10° to the northwest of its position in the control experiment (Fig. 4a), which still places it close to the (now absent) Altiplano. Thus, *the proximity of the Bolivian high to the Altiplano should not be interpreted as a causal relationship.*

According to the linear model analysis, the position of the Bolivian high is largely explained by the presence of Amazonian precipitation to the northeast. In the no-Andes experiment, this precipitation maximum (Fig. 9) is shifted about 5° equatorward but is significantly stronger than in the control experiment (Fig. 5c), resulting in an only slightly weakened vortex stretching term (not shown). And while the central Andes precipitation maximum is now absent, the SACZ has shifted significantly to the west. This combination of relatively unchanged vortex stretching over the Amazon basin and a westward shift in the SACZ results in little overall change in the position of the Bolivian high.

The circulation about the Bolivian high is weaker in

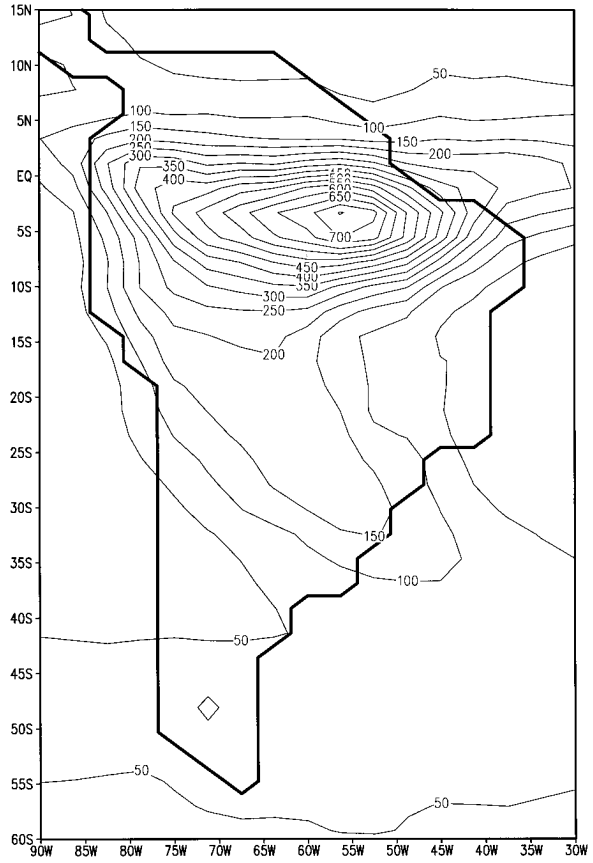

FIG. 9. As in Fig. 5c (and Fig. 5d) but from the no-Andes experiment.

the absence of the Andes, especially to the north of the high, where the easterlies have been reduced by 5–10 m s^{-1} (Figs. 8a and 4a). The linear model response to central Andean condensational heating (Fig. 7f) suggests that this weakening is due to the absence of strong precipitation in the central Andes, but the equatorward shift of the Amazonian precipitation may also be a factor. To the northeast of the Bolivian high, southerly to southwesterly winds (Fig. 8a) replace the southeasterlies of the control integration (Fig. 4a). Associated with this is a southward shift of the Nordeste low, which has opened up into a deep trough. The formation of high pressure to the south of the Nordeste low as a result of condensational heating in the SACZ (Fig. 7g) indicates that the deepening of the trough in the no-Andes experiment is associated with the westward shift of the SACZ. The westerly flow to the north of this trough, which can be interpreted as a Kelvin wave response to Amazonian precipitation (Silva Dias et al. 1983; DeMaria 1985), has strengthened in association with the stronger and equatorward-shifted rainfall maximum in the Amazon.

The vertical structure of the Bolivian high is relatively unaffected by the removal of the Andes (Figs. 8b and 4b). However, the weakening of the circulation is again evident, as is the deepening of the trough to the east. These differences are also readily apparent in the 200-mb eddy geopotentials (Figs. 8c and 4c) and 400-mb eddy temperatures (Figs. 8d and 4d). The proposed connection between the westward shift of the SACZ and the lowering of upper-level pressure and temperature to the east–southeast of the Bolivian high is made further evident in these figures. In addition, the mechanically induced, midlatitude trough in the lee of the Andes (Fig. 4c) is, understandably, absent in Fig. 8c.

6. Steady-state dynamics and thermodynamics of the Bolivian high

To understand the dynamic and thermodynamic balances that characterize the Bolivian high, the climatological vorticity and thermodynamic budgets of the no-Andes GCM experiment are examined. This experiment has an advantage over the observations (and the GCM control experiment) in that sigma-to-pressure interpolation errors are greatly minimized over South America, due to the absence of the Andes. This significantly reduces the amount of small-scale noise that appears in the budget terms. The essential physics associated with the Bolivian high is still present in the no-Andes experiment, since the high is generated over the flat continent and only modified by the presence of topography.

a. Upper-level vorticity budget

The climatological vorticity equation in pressure coordinates is given by

$$\overline{\frac{\partial \zeta}{\partial t}} + \overline{\mathbf{v}\cdot\nabla(\zeta + f)} + \overline{\omega\frac{\partial \zeta}{\partial p}} = \overline{-(\zeta + f)\nabla\cdot\mathbf{v}} - \overline{\left(\frac{\partial \omega}{\partial x}\frac{\partial v}{\partial p} - \frac{\partial \omega}{\partial y}\frac{\partial u}{\partial p}\right)} + \overline{F}, \quad (1)$$

where ζ is relative vorticity, $\mathbf{v} = (u,v)$ is horizontal wind velocity, ω is vertical p-velocity, and f is the Coriolis parameter. Here F represents the effects of subgrid-scale momentum transports, and overbars denote climatological means (averaged over the length of the GCM integration). The vorticity tendency term is negligible, so (1) becomes

$$0 = -\overline{\mathbf{v}}\cdot\nabla(\overline{\zeta} + f) - \overline{\omega}\frac{\partial \overline{\zeta}}{\partial p} - (\overline{\zeta} + f)\nabla\cdot\overline{\mathbf{v}} - \left(\frac{\partial \overline{\omega}}{\partial x}\frac{\partial \overline{v}}{\partial p} - \frac{\partial \overline{\omega}}{\partial y}\frac{\partial \overline{u}}{\partial p}\right) + \overline{F} + \overline{\delta}_\zeta, \quad (2)$$

where δ_ζ denotes the vorticity tendency due to the transient eddies. At 200 mb in the GCM, the tilting and vertical advection of mean relative vorticity over South America is roughly an order of magnitude smaller than

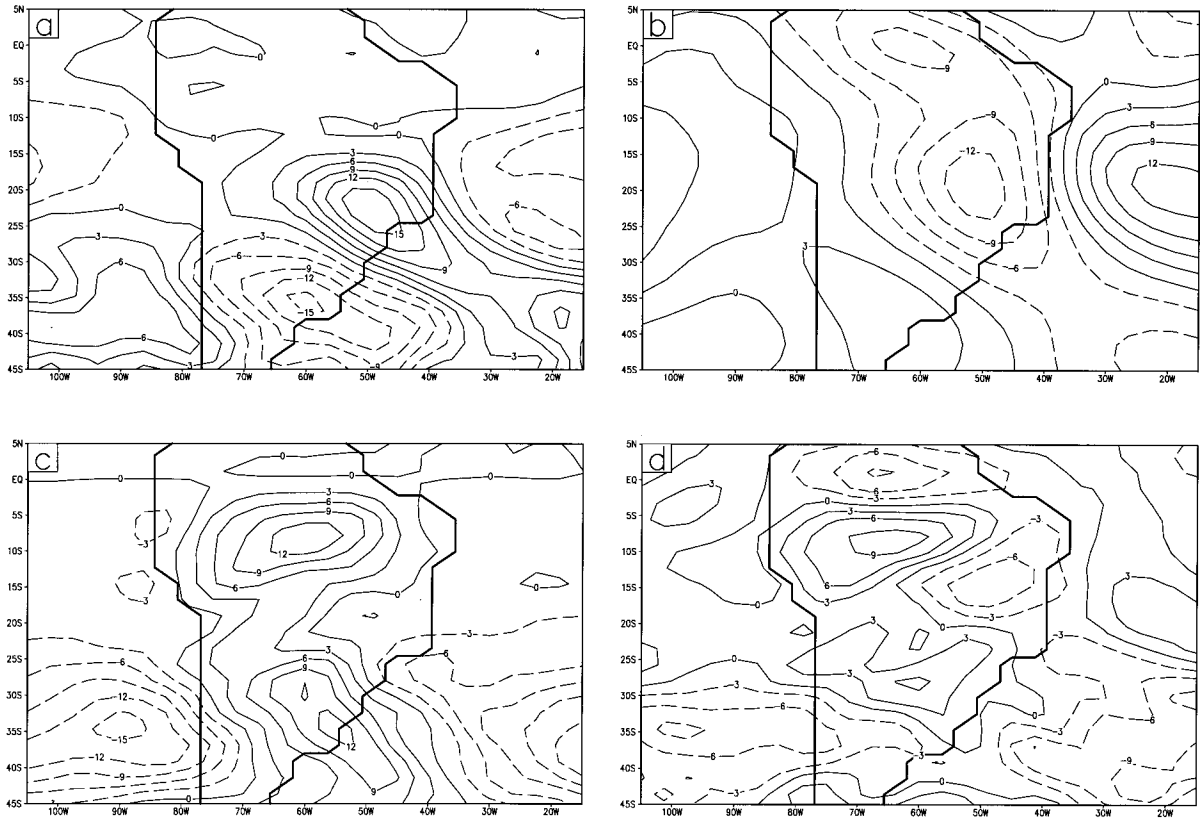

FIG. 10. Terms from the 200-mb vorticity budget [Eq.(3)] of the no-Andes experiment, including (a) $-\overline{\mathbf{v}}\cdot\boldsymbol{\nabla}\overline{\zeta}$, (b) $-\beta\overline{v}$, (c) $-f\overline{D}$, and (d) the sum of the three. Contour interval is 3×10^{-11} s^{-2}, and negative values are dashed.

the largest terms. The stretching of mean relative vorticity is also small (about a factor of 4 smaller than the largest terms), and turbulent fluxes are identically zero at 200 mb in the GCM. The transients are generally small but are not negligible in all regions; they will be neglected for the time being. Thus, (2) reduces to an approximate balance between the horizontal advection of absolute vorticity and the stretching of planetary vorticity,

$$0 \approx -\overline{\mathbf{v}}\cdot\boldsymbol{\nabla}\overline{\zeta} - \beta\overline{v} - f\overline{D}, \tag{3}$$

where

$$\beta = \frac{df}{dy} \quad \text{and} \quad D = \boldsymbol{\nabla}\cdot\mathbf{v}.$$

Each term in (3) is shown in Fig. 10, along with the sum of the three terms. There are clearly some regions where Eq. (3) is not a good approximation (Fig. 10d), particularly along 65°W between 5°N and 15°S. Most of the residual in Fig. 10d is associated with the net vorticity transients $\overline{\delta_\zeta}$. This term is composed of a number of individual components, many of which significantly offset each other, making the interpretation of the vorticity transients rather involved and of questionable relevance. For this reason, the following discussion focuses on three regions where the transients are of secondary importance, namely the eastern Amazon basin, the SACZ, and throughout the Nordeste low (i.e., the trough in Fig. 8a).

The advection of relative vorticity is small north of about 15°S (Fig. 10a), so in the vicinity of the maximum Amazonian precipitation (Fig. 9) and extending southwest into the northern SACZ, Eq. (3) simplifies to an approximate balance between the advection (Fig. 10b) and stretching (Fig. 10c) of planetary vorticity: $\beta\overline{v} \approx -\overline{fD}$. (The NASA/DAO observations show a similar balance in the eastern Amazon basin down to about 20°S. This approximation does not hold, however, to the west of the Amazonian precipitation, where most of the vorticity stretching is balanced by the transients.) On an equatorial β-plane, this expression becomes

$$\overline{v} \approx -y\overline{D}, \tag{4}$$

where y is the distance from the equator. This simple Sverdrup balance represents the fundamental dynamics of steady-state Gill models (e.g., Gill 1980; DeMaria 1985) and has been utilized to explain characteristics of the tropical circulation. Equation (4) indicates that horizontal divergence is associated with equatorward meridional velocity that maximizes poleward of the divergence maximum. Thus, assuming approximate geostrophy, upper-level divergence maxima in the Southern

Hemisphere are bounded on the southwest by high pressure and on the southeast by low pressure. This explains the positioning of the Bolivian high (Nordeste low) to the southwest (southeast) of the Amazonian precipitation maximum. Also quantified in Eq. (4) is the previously noted stronger response in higher latitudes (given the same forcing). Hence, the vortex stretching mechanism in the SACZ is just as strong as in the Amazon (Fig. 10c), even though the upper-level divergence (and precipitation) is weaker. Similar interpretations of the tropical circulation have been offered before by Gill (1980) and Phlips and Gill (1987).

In the central and southern portions of the SACZ, the strong stretching of planetary vorticity at 200 mb (Fig. 10c) is predominately balanced by relative vorticity advection (Fig. 10a) instead of planetary vorticity advection (as in the Amazon and northern SACZ). A similar balance occurs about 30° west of the SACZ in a region of convergence, but there the transients are not negligible. Almost all of the advection is zonal in nature, so (3) simplifies to

$$\frac{\partial \overline{\zeta}}{\partial x} \approx -\frac{f\overline{D}}{\overline{u}}, \tag{5}$$

and upper-level divergence associated with the SACZ is bounded by higher (lower) relative vorticity to the east (west). The NASA/DAO observations show a similar pattern south of 25°S, not only in the SACZ, but also in other regions of upper-level divergence or convergence. This is illustrated in Fig. 3, which shows regions of maximum (minimum) relative vorticity located downstream from regions of maximum divergence (convergence).

In the vicinity of the Nordeste low (Fig. 8a), where vortex stretching is minimal (Fig. 10c), an approximate balance exists between the advection of relative (Fig. 10a) and planetary (Fig. 10b) vorticity. This constitutes conservation of absolute vorticity following the steady horizontal flow field, a feature of this region that is also evident in the NASA/DAO data and has been previously noted by Sardeshmukh and Hoskins (1985). In contrast to Sardeshmukh and Hoskins (1985), however, we find that a linearization of the relative vorticity advection about the zonal mean basic state is appropriate for this region. This supports the results of the linear model in indicating that nonlinearities are not crucial for a good simulation of the Nordeste low.

b. Thermodynamic considerations

1) MAINTENANCE OF THE WARM CORE

Given that the Bolivian high is a response to midtropospheric condensational heating, it is clear that this heating is responsible for the high's warm core. However, the details of this connection are not at all obvious, given that the warm core (Fig. 8d) is located considerably to the southwest of the heating maximum (Fig. 9). The steady-state dynamics of this southwestward positioning have been explained in terms of the Sverdrup balance, from which one can obtain the temperature field, assuming geostrophy, continuity, and hydrostatic balance. It would, however, be more appealing to explain the anomalous temperature field in terms of the heating itself.

The climatological thermodynamic equation in pressure coordinates is given by

$$\frac{\overline{\partial T}}{dt} + \overline{\mathbf{v}\cdot\boldsymbol{\nabla} T} + \overline{\omega\frac{\partial T}{\partial p}} = \frac{\overline{Q}}{c_p} + \overline{\omega\frac{RT}{c_p p}}, \tag{6}$$

where T is temperature and Q is diabatic heating rate. The climatological temperature tendency is negligible, and if we also ignore the transient terms for the time being, (6) becomes

$$0 \approx \frac{\overline{Q}}{c_p} + \overline{\omega}\left(\frac{R\overline{T}}{c_p p} - \frac{\partial \overline{T}}{\partial p}\right) + \left[-\overline{u}\frac{\partial \overline{T}}{\partial x} - \overline{v}\frac{\partial \overline{T}}{\partial y}\right]. \tag{7}$$

According to (7), the Bolivian high's warm core is maintained against cold-air advection [the bracketed term in Eq.(7)] by an imbalance of the first two terms on the rhs of the equation. In the Tropics this imbalance is very delicate, as the diabatic heating and adiabatic cooling terms nearly cancel. Indeed, an exact balance is often assumed in order to obtain a diagnostic relationship for the vertical velocity, in which case information about the temperature anomaly must be obtained through the dynamics. However, the Bolivian high's warm core extends well into the subtropics, where winds and temperature gradients are strong enough to provide a robust analysis of Eq. (7).

Figure 11 shows the three terms on the rhs of (7) as well as their sum. The fields are shown at 400 mb, where the warm core reaches a maximum in the no-Andes experiment (Fig. 8b). The diabatic heating field (Fig. 11a) is comprised of condensational heating and radiative cooling, which are the only significant sources of diabatic heating at this level. A region of strong subsidence to the southwest of the Bolivian high (centered around 30°S, 90°W) is associated with significant adiabatic warming (Fig. 11b), which is not entirely compensated by radiative cooling (Fig. 11a). Instead, this net heating is balanced by cold-air advection (Fig. 11c). About 30° to the east of this region, condensational heating in the SACZ is insufficient to balance the cooling associated with rising air and radiation. Thus, net cooling occurs, which is balanced by warm-air advection.

The implications of Fig. 11 for the maintenance of the warm core can be better understood by adopting a Lagrangian perspective, in which the horizontal temperature advection term in (7) is brought to the lhs and interpreted as the rate of change of temperature following the mean horizontal flow field. It is also advantageous to expand the temperature field into its eddy and

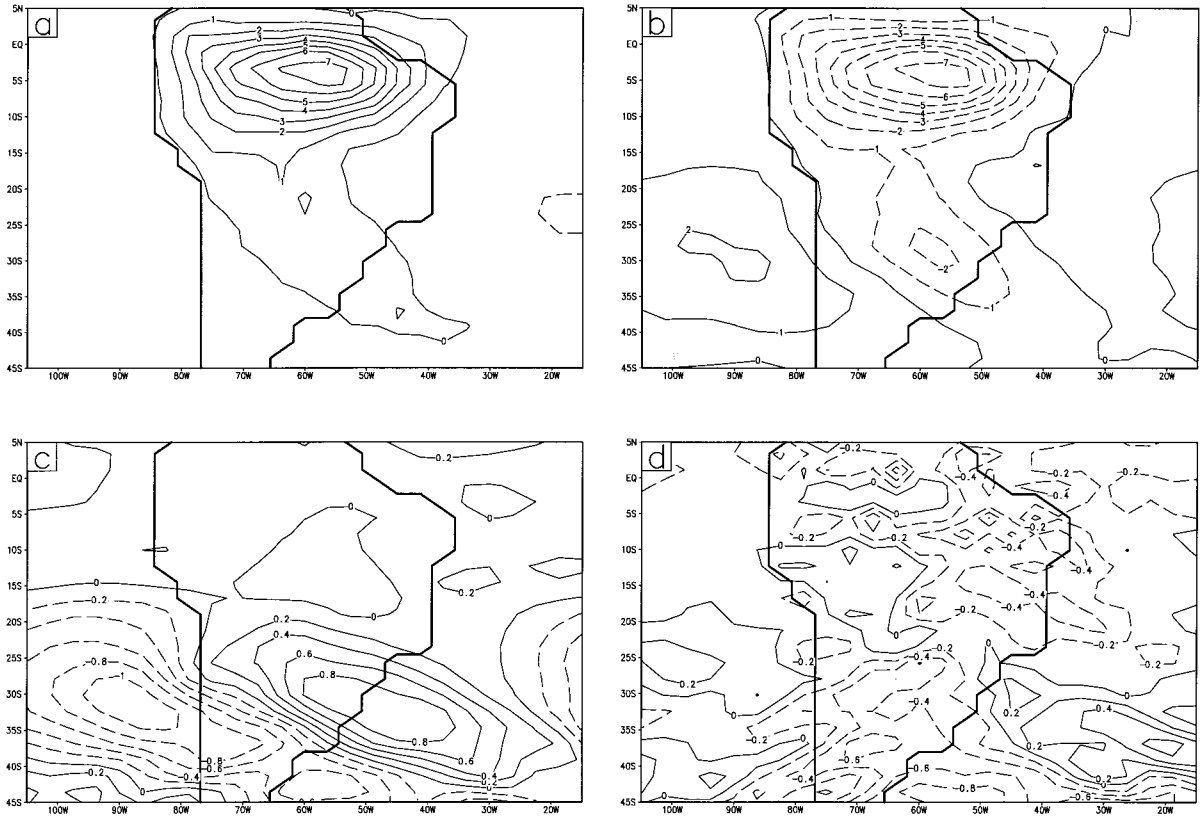

FIG. 11. Terms from the 400-mb thermodynamic budget [Eq.(7)] of the no-Andes experiment, including (a) $(\overline{Q}/c_p)$, (b) $\overline{\omega}[(R\overline{T}/c_p p) - (\partial\overline{T}/\partial p)]$, (c) $-\overline{u}(\partial\overline{T}/\partial x) - \overline{v}(\partial\overline{T}/\partial y)$, and (d) the sum of the three. Contour intervals are 1 K day^{-1} in (a) and (b) and 0.2 K day^{-1} in (c) and (d).

zonal mean components (denoted by * and [], respectively), yielding

$$\frac{\overline{dT}^*}{dt} \approx \frac{\overline{Q}}{c_p} + \overline{\omega}\left(\frac{R[\overline{T}]}{c_p p} - \frac{\partial[\overline{T}]}{\partial p}\right), \tag{8}$$

where $(\overline{d}/dt) = \overline{u}(\partial/\partial x) + \overline{v}\,(\partial/\partial y)$. [In deriving Eq. (8) the terms $\overline{v}\,(\partial[\overline{T}]/\partial y)$ and $\overline{\omega}\,[(RT^*/c_p p) - (\partial\overline{T}^*/\partial p)]$ have been neglected, as they do not play a significant role.] The balance in (8) is illustrated in Fig. 12, which shows the 400-mb wind and eddy temperature fields superimposed on the net ''heating'' field [the rhs of Eq. (8)]. Since the flow south of 15°S is primarily westerly, warm (cold) temperature anomalies can be attributed to net heating (cooling) to the west of the anomaly. In other words, *a large portion of the Bolivian high's warm core is maintained by strong subsidence off the west coast of South America, not through the direct effects of condensational heating.* In a similar manner, the anomalously cold temperatures associated with subtropical portions of the Nordeste low are related to net cooling in the SACZ, where rising motion is too strong to balance the net diabatic heating. This interpretation applies throughout the mid to upper levels of the warm core (roughly 550–250 mb), south of about 15°S. In the lower levels, turbulent heat flux, transient eddies, and a weaker wind field complicate the picture considerably, while north of 15°S the horizontal temperature advection (Fig. 11c) is too weak to provide a robust analysis.

To relate this discussion to previous modeling studies of the Bolivian high, consider a linearized form of (8) that neglects all but the three most important terms:

$$[\overline{u}]\frac{\partial\overline{T}^*}{\partial x} \approx \frac{\overline{Q}^*}{c_p} + \overline{\omega}^*\left(\frac{R[\overline{T}]}{c_p p} - \frac{\partial[\overline{T}]}{\partial p}\right). \tag{9}$$

Equation (9) succinctly states that, in the presence of westerly flow, the warm core is associated with net heating to the west (in this case, adiabatic warming). In contrast, a steady-state Gill model linearized about a basic state at rest (e.g., DeMaria 1985) has $[u] = 0$ and the lhs of (9) is replaced with a Newtonian cooling term, $\alpha\overline{T}^*$. Thus, the formulation of the Gill model implies (unrealistically) that the net heating anomaly is coincident with the temperature anomaly. [In a time-dependent Gill model, the lhs of (9) is replaced by the temperature tendency term, suggesting that the heating imbalance on the rhs of (9) is also important for the propagation characteristics of the Bolivian high.]

The presence of pronounced subsidence off the west

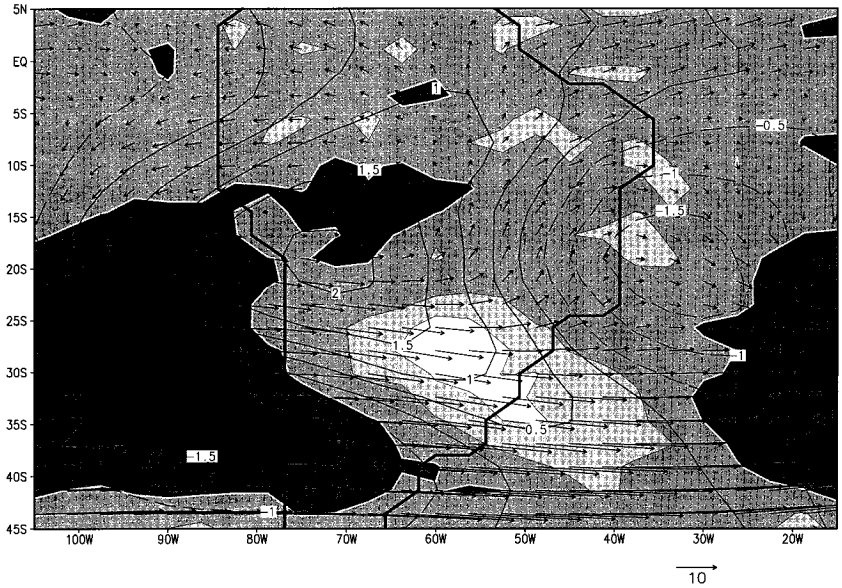

FIG. 12. 400-mb wind vectors (10 m s^{-1} shown in lower right corner) and eddy temperature (0.5 K interval, negative contours dashed) from the no-Andes experiment. Net heating rates [the rhs of Eq. (8)] are shown shaded (0.5 K day^{-1} interval), with the zero contour in white. Darker (lighter) shading indicates net heating (cooling).

coast of South America is noted in the observational study of Virji (1981) and is implied by the upper-level wind convergence in the NASA/DAO data (Fig. 3b). Modeling studies (DeMaria 1985; Gandu and Geisler 1991) have shown strong sinking motion to the west of the Bolivian high in response to imposed Amazonian heating, suggesting that precipitation in the Amazon is the primary forcing for this subsidence. It is likely, however, that precipitation in the central Andes and SACZ also plays a role. In the control experiment, for example, adiabatic warming at 30°S, 90°W is even stronger than in the no-Andes experiment, and a secondary maximum is present along the western flank of the central Andes (20°S, 75°W).

There is evidence in the NASA/DAO data that the modeled cold-air advection off the west coast is an observed feature. Gutman and Schwerdtfeger (1965) also found cold-air advection to the west of the Bolivian high and suggested that this advection is balanced by sensible and latent heating over the Altiplano. However, their measurements were made from radiosonde data at Antofagasta on the west coast of Chile, so the advection they measured may be balancing strong subsidence along the west coast, not diabatic heating over the Altiplano.

2) ORIGIN OF THE COLD CAPPING LAYER

Both the observations (Fig. 2b) and the no-Andes experiment (Fig. 8b) show that the Bolivian high is capped by a cold layer that maximizes around 100 mb. A warm layer is present above the Nordeste low, also with a maximum near 100 mb. The source of these anomalies is adequately described by (8), as illustrated in Fig. 13, which shows wind vectors and eddy temperature contours at 100 mb, superimposed on the rhs of (8). At this level, the winds north of 25°S are primarily easterly and diabatic heating rates are small. Thus, the cold (warm) anomaly above the Bolivian high (Nordeste low) is primarily the result of adiabatic cooling (warming) to the east of the temperature anomaly. The cooling process can be thought of as large-scale convective ''overshooting,'' where the vertical velocity remains significant well above the level at which condensational heating becomes negligible. This is similar to the interpretations offered by Gutman and Schwerdtfeger (1965) and Kreuels et al. (1975). However, we wish to emphasize that the large-scale overshooting in the GCM is not coincident with the Bolivian high and the cold anomaly (which it would be in a steady-state Gill model). Instead, the cold anomaly is positioned roughly 15°–20° to the west of the overshooting as a result of westward temperature advection. The NASA/DAO observations are broadly consistent with these model results.

3) THERMAL TRANSIENTS

So far the effects of the thermal transients have not been considered in this analysis. However, results from the linear model indicate that the thermal transients partially offset the effects of condensational heating and weaken the Bolivian high (at least at $\sigma = 0.34$). The

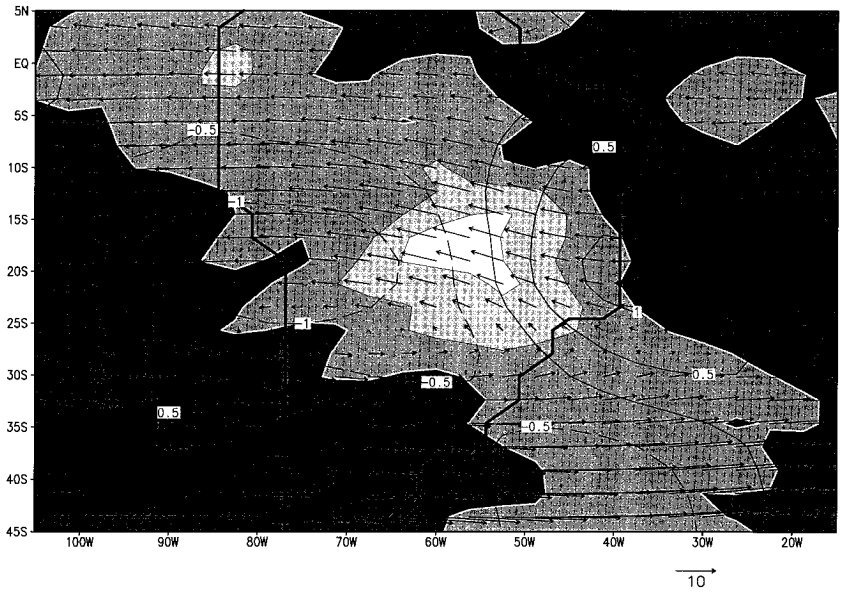

FIG. 13. As in Fig. 12 but at 100 mb. Shaded contour interval is 1 K day^{-1}.

climatological temperature tendency due to transient eddies $\overline{\delta_T}$ can be partitioned as

$$\overline{\delta_T} = -\overline{\mathbf{v}' \cdot \nabla T'} - \overline{\omega' \frac{\partial T'}{\partial p}} + \overline{\omega' \frac{RT'}{c_p p}}, \qquad (10)$$

where primes denote deviations from the time mean. In the no-Andes experiment, the last term on the rhs. of (10) is negligible. Figure 14 shows the two remaining transient terms, horizontal and vertical temperature advection, vertically averaged below (Figs. 14a and 14b) and above (Figs. 14c and 14d) the level of the Bolivian high's warm core.

Below 400 mb the thermal transients have a net cooling effect over most of the South American continent. In the SACZ and midlatitudes, the cooling is dominated by transient horizontal temperature advection (Fig. 14a) in association with propagating cold fronts, which are commonly observed features of the SACZ (Kousky 1979; Kodama 1992). In the Amazon and northern SACZ, the transient vertical temperature advection term is dominant (Fig. 14b) and exhibits structure very similar to the precipitation field itself (Fig. 9). Most of the linear model response to the thermal transients (Fig. 7c) is associated with this term, and its structural similarity to the condensational heating field helps to explain the compensating effect of the thermal transients in the linear model.

Above the Bolivian high's warm core, transient horizontal temperature advection (Fig. 14c) is considerably weaker in the SACZ, especially to the north. More importantly, the vertical advection term (Fig. 14d) is now stronger and provides net *heating* throughout the Amazon region and the SACZ. This vertical structure in the transient vertical temperature advection (cooling below 400 mb, heating above) has the important effect of raising the net vertical heating profile in the GCM. In fact, above 300 mb the temperature tendency due to the transients exceeds the diabatic heating rate, and most of the adiabatic cooling in the Amazon region is balanced by thermal transients. Correspondingly, above about 250 mb the linear model geopotential response to thermal transient forcing is such that the effects of condensational heating are bolstered rather than offset. This response maximizes around 170 mb, where circulation features resembling the Bolivian high and Nordeste low are simulated. These features are not strong enough, however, to compensate for the linear model's tendency to place the maximum condensational heating response at 350 mb. Thus, nonlinearities still play an important role in determining the vertical structure.

In the GCM the transient vertical advection of temperature is important not only over the Amazon and SACZ, but also in other tropical regions with high precipitation rates. This suggests that in such regions the vertical velocity and temperature lapse rate are significantly correlated [see the second term in Eq. (10)]. In other words, below 400 mb (Fig. 14b), episodes of anomalous upward (downward) vertical motion are associated with a decreased (increased) lapse rate, while above 400 mb (Fig. 14d), the opposite is true. This correlation is also evident in the NASA/DAO observations, except that the vertical node occurs at 300 mb (the level of the warm core in the observations). One possible explanation for this correlative relationship is that anomalous upward vertical motion usually occurs during strong convective events, which release anomalous latent heat and produce a stronger than normal warm core (i.e., decreased lapse rates below the warm core and increased lapse rates above).

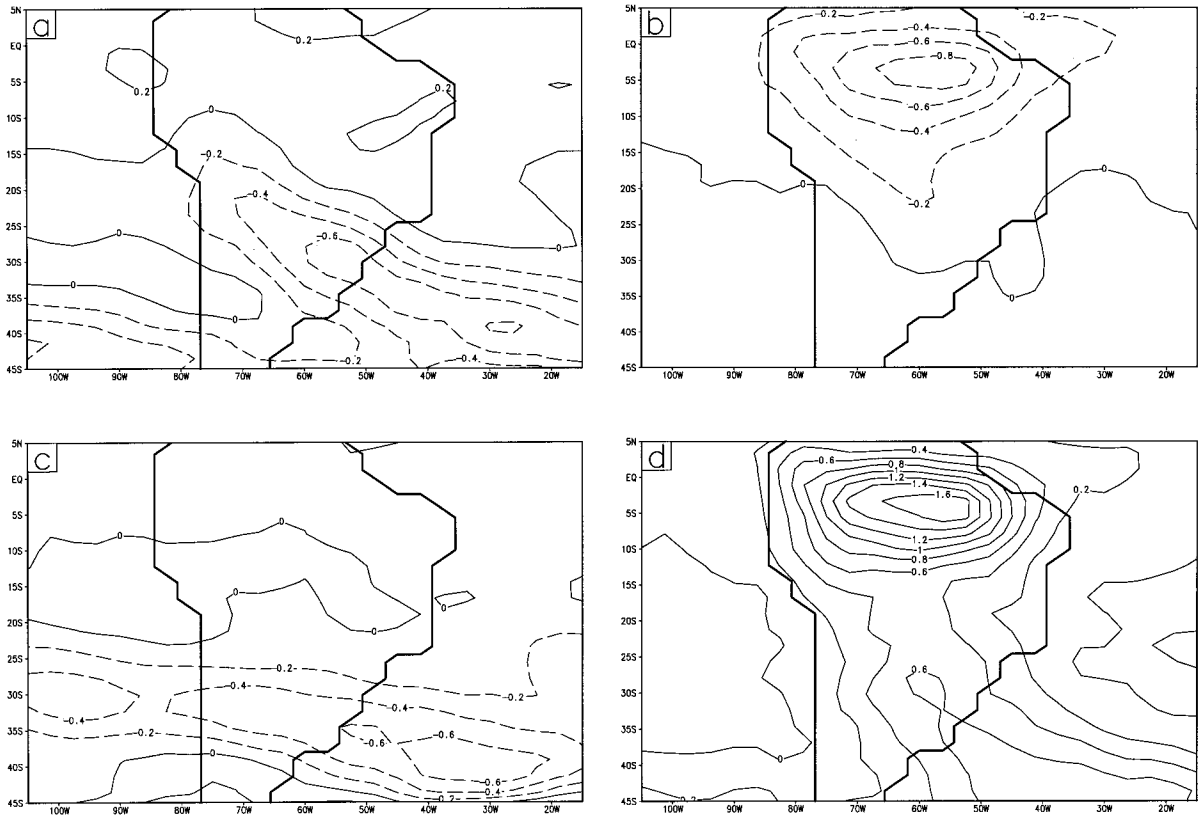

FIG. 14. (a) Horizontal and (b) vertical temperature advection by the transient eddies in the no-Andes experiment, averaged from the surface to 450 mb. Contour interval is 0.2 K day^{-1}. (c) and (d) As in (a) and (b), respectively, but averaged from 350 mb to 170 mb.

7. Summary and conclusions

In this study we explore the mechanisms responsible for the structure in the upper-tropospheric circulation over South America during austral summer. The principal focus is the Bolivian high, a prominent warm-core anticyclone that establishes itself over the elevated Altiplano of the central Andes. Other climatological features of interest include the cold-core Nordeste low to the east of the high, as well as a weak extratropical trough over the western Atlantic. Previous observational and modeling studies are reviewed to summarize the important features of the upper-level circulation and our current understanding of them.

An R30, 30-level GCM is used to generate a realistic simulation of the Bolivian high and associated circulation features. Some discrepancies with observations are noted, including a stronger and zonally elongated Bolivian high and weak sensible heat fluxes over the Altiplano. In general, however, the agreement is good, and the GCM reproduces reasonable structure in the wind, temperature, and heating fields over South America. A GCM experiment without Andean topography and a linearized version of the GCM are used to determine how the upper-level circulation features are generated. In particular, the individual roles of diabatic heating, transient eddies, and mechanical topographic forcing are identified, as well as the indirect effects of topography through modifications of the diabatic heating field. Much of the structure is reproduced in the absence of the Andes, allowing a diagnosis of the dynamics and thermodynamics of the circulation features in a simpler framework.

The majority of the structure in the upper-tropospheric summertime circulation over South America is associated with condensational heating. The Bolivian high represents a collective response to precipitation in the Amazon, central Andes, and SACZ, with its position over the Altiplano being largely the result of Amazonian precipitation to the northeast, and its strength most strongly influenced by precipitation rates in the central Andes. Even though condensational heating rates in the SACZ are relatively weak, stronger vortex stretching results in a significant response in this region, most notably an extension of the Bolivian high to the southeast.

The only direct, mechanical effect of the Andes mountains on the upper-level circulation is a weak lee trough in midlatitudes. Sensible heating over the Altiplano generates a shallow monsoonal circulation that has little direct impact on the upper-tropospheric circulation. On the other hand, the Andes indirectly strengthen the Bolivian high by inducing precipitation

in the central Andes and modifying precipitation elsewhere. Despite these important effects on the diabatic heating field, however, the role of topography remains secondary, as evidenced by the presence of a well-defined Bolivian high in the absence of the Andes.

The positioning of the Bolivian high to the southwest of the Amazon basin can be understood by examining the upper-level vorticity and thermodynamic budgets. Upper-tropospheric divergence over the Amazon is predominantly balanced by the advection of planetary vorticity (a Sverdrup balance), implying equatorward flow south of the divergence maximum and high pressure to the west. The positioning of the high's warm core is largely explained by the presence of compensatory subsidence off the subtropical west coast of South America. The adiabatic warming associated with this subsidence is not completely offset by radiative cooling and, in the presence of westerly flow, forms a warm anomaly to the east of the subsidence. In a similar fashion, the layer of cold air above the Bolivian high forms west of the precipitation in association with large-scale convective overshooting above the Amazon basin. This adiabatic cooling is embedded in easterly flow, thereby placing the cold layer to the west of the overshooting.

The Nordeste low is successfully simulated as a direct, linear response to condensational heating. This result is in contrast to previous studies, which did not consider the significance of remote precipitation. In particular, the inclusion of African precipitation is required (in conjunction with Amazonian precipitation) to form a deep trough to the east of the Bolivian high, while the SACZ ''pinches'' the trough into a closed Nordeste low. The structure of this closed low is moderately affected by the Andes, primarily through the influence of topography on the longitudinal position of the SACZ. Placement of the Nordeste low to the east of the Amazonian precipitation can be explained by a Sverdrup balance, and the low's cold core is at least partly maintained by net cooling in the SACZ. The flow field surrounding the Nordeste low approximately conserves absolute vorticity, suggesting that it is important to include a nonzero basic-state flow when modeling this feature; however, full nonlinearity is not necessary.

Nonlinearities are important, however, for simulating the vertical structure of the Bolivian high. The linear model simulates the Bolivian high's warm core at about 500 mb, considerably lower than the GCM's 400 mb (300 mb in the observations). This indicates the significance of nonlinearities in raising the vertical response to condensational heating. (The discrepancy between the GCM and observational heating profiles is thought to be largely due to the GCM's moist convective adjustment.) The transient vertical advection of temperature, which transports anomalous heat above the warm core during periods of intense convection, is especially important in this regard and should not be overlooked when examining the upper-tropospheric, climatological heat budget in regions of high precipitation.

Many avenues of further research are indicated in this study. Conclusions regarding the effects of the Andes are preliminary, and a more realistic investigation of their influence is needed. In particular, a model (perhaps mesoscale) that successfully incorporates the full height of the Andes and the sensible heating effects of the Altiplano (through improved land surface conditions) would be especially beneficial. It would also be useful to understand the effects of model simplifications made in this study, such as fixed clouds and the lack of diurnal and seasonal cycles, as well as the use of simple parameterizations such as moist convective adjustment. A climatological study such as this one also does not provide an understanding of the transient nature of features such as the Bolivian high and Nordeste low. For example, how do the Andes affect the timing of the annual cycle of convective activity over South America, including the formation and demise of the Bolivian high and Nordeste low? Observational studies detailing the variability of these features and how they relate to other aspects of the South American climate (Amazonian precipitation, west coast subsidence, SACZ frontal activity, etc.) would also represent valuable contributions.

Acknowledgments. The authors wish to thank two anonymous reviewers for constructive criticism on the original manuscript. Acknowledgment is made to the National Center for Atmospheric Research, which is sponsored by the National Science Foundation, for the computing time used in this research. Data used by the authors in this study include data produced through funding from the Earth Observing System of NASA's Mission to Planet Earth in cooperation with the National Oceanic and Atmospheric Administration. The data were provided by the Earth Observing System Data and Information System Distributed Active Archive Center at Goddard Space Flight Center which archives, manages, and distributes this dataset. Figures were produced using the Grid Analysis and Display System provided by the Center for Ocean–Land–Atmosphere Interactions at the University of Maryland. This work represents a portion of J. D. Lenters' PhD dissertation at Cornell University and was supported by NASA Grant NAGW-2638 and NSF Grant ATM-9300311.

REFERENCES

Aceituno, P., and A. Montecinos, 1993: Circulation anomalies associated with dry and wet periods in the South American Altiplano. Preprints, *Proc. Fourth Int. Conf. on Southern Hemisphere Meteorology*, Hobart, Australia, Amer. Meteor. Soc., 330–331.

Boffi, J. A., 1949: Effect of the Andes Mountains on the general circulation over the southern part of South America. *Bull. Amer. Meteor. Soc.*, **30,** 242–247.

Broccoli, A. J., and S. Manabe, 1992: The effects of orography on midlatitude Northern Hemisphere dry climates. *J. Climate,* **5,** 1181–1201.

DeMaria, M., 1985: Linear response of a stratified tropical atmosphere to convective forcing. *J. Atmos. Sci.,* **42,** 1944–1959.

Figueroa, S. N., P. Satyamurty, and P. L. Silva Dias, 1995: Simulations of the summer circulation over the South American region with an eta coordinate model. *J. Atmos. Sci.,* **52,** 1573–1584.

Flohn, H., 1968: Contributions to a meteorology of the Tibetan Highlands. Atmos. Sci. Paper 130, 120 pp. [Available from Colorado State University, Department of Atmospheric Science, Fort Collins, CO 80523.]

Gandu, A. W., and J. E. Geisler, 1991: A primitive equations model study of the effect of topography on the summer circulation over tropical South America. *J. Atmos. Sci.,* **48,** 1822–1836.

Gill, A. E., 1980: Some simple solutions for heat-induced tropical circulation. *Quart. J. Roy. Meteor. Soc.,* **106,** 447–462.

——, and P. J. Phlips, 1986: Nonlinear effects on heat-induced circulation of the tropical atmosphere. *Quart. J. Roy. Meteor. Soc.,* **112,** 69–91.

Gutman, G. J., and W. Schwerdtfeger, 1965: The role of latent and sensible heat for the development of a high pressure system over the subtropical Andes, in the summer. *Meteor. Rundsch.,* **18,** 69–75.

Hahn, D. G., and S. Manabe, 1975: The role of mountains in the South Asian monsoon circulation. *J. Atmos. Sci.,* **32,** 1515–1541.

Hastenrath, S., 1991: *Climate Dynamics of the Tropics.* Kluwer Academic Publishers, 488 pp.

Horel, J. D., A. N. Hahmann, and J. E. Geisler, 1989: An investigation of the annual cycle of convective activity over the tropical Americas. *J. Climate,* **2,** 1388–1403.

Kessler, A., 1981: Fluctuations of the water budget on the Altiplano and of the atmospheric circulation (in German). *Aachener Geographische Arbeiten,* **14,** 111–122.

Kleeman, R., 1989: A modeling study of the effect of the Andes on the summertime circulation of tropical South America. *J. Atmos. Sci.,* **46,** 3344–3362.

Kodama, Y.-M., 1992: Large-scale common features of subtropical precipitation zones (the Baiu Frontal Zone, the SPCZ, and the SACZ). Part I: Characteristics of subtropical frontal zones. *J. Meteor. Soc. Japan,* **70,** 813–835.

——, 1993: Large-scale common features of sub-tropical convergence zones (the Baiu Frontal Zone, the SPCZ, and the SACZ). Part II: Conditions of the circulations for generating the STCZs. *J. Meteor. Soc. Japan,* **71,** 581–610.

Kousky, V. E., 1979: Frontal influences on Northeast Brazil. *Mon. Wea. Rev.,* **107,** 1140–1153.

——, and M. A. Gan, 1981: Upper tropospheric cyclonic vortices in the tropical South Atlantic. *Tellus,* **33,** 538–550.

——, and M. T. Kagano, 1981: A climatological study of the tropospheric circulation over the Amazon region. *Acta Amazonica,* **11,** 743–758.

Kreuels, R., K. Fraedrich, and E. Ruprecht, 1975: An aerological climatology of South America. *Meteor. Rundsch.,* **28,** 17–24.

Legates, D. R., and C. J. Willmott, 1990: Mean seasonal and spatial variability in gauge-corrected, global precipitation. *Int. J. Climatol.,* **10,** 111–127.

Lenters, J. D., 1997: Climate dynamics of South America during summer: Connections between the large-scale circulation and regional precipitation. Ph.D. dissertation, Cornell University, 268 pp.

——, and K. H. Cook, 1995: Simulation and diagnosis of the regional summertime precipitation climatology of South America. *J. Climate,* **8,** 2988–3005.

Manabe, S., 1969: Climate and the ocean circulation. The atmospheric circulation and the hydrology of the earth's surface. *Mon. Wea. Rev.,* **97,** 739–744.

Matsuno, T., 1966: Quasi-geostrophic motions in the equatorial area. *J. Meteor. Soc. Japan,* **44,** 25–43.

Nishizawa, T., and M. Tanaka, 1983: The annual change in the tropospheric circulation and the rainfall in South America. *Arch. Meteor. Geophys. Bioklimatol. Ser. B,* **33,** 107–116.

Phlips, P. J., and A. E. Gill, 1987: An analytical model of the heat-induced tropical circulation in the presence of a mean wind. *Quart. J. Roy. Meteor. Soc.,* **113,** 213–236.

Rao, G. V., and H. van de Boogaard, 1986: A comparison between the Bolivian and Tibetan upper anticyclones. Preprints, *Proc. Second Int. Conf. on Southern Hemisphere Meteorology,* Wellington, New Zealand. Amer. Meteor. Soc., 278–279.

——, and S. Erdogan, 1989: The atmospheric heat source over the Bolivian plateau for a mean January. *Bound.-Layer Meteor.,* **46,** 13–33.

Rooney, D. M., and G. S. Janowitz, 1979: Flow over the Rocky and Andes Mountains: Application of an analytical model. *J. Atmos. Sci.,* **36,** 549–558.

Sardeshmukh, P. D., and B. J. Hoskins, 1985: Vorticity balances in the tropics during the 1982–83 El Niño–Southern Oscillation event. *Quart. J. Roy. Meteor. Soc.,* **111,** 261–278.

Satyamurty, P., R. P. Santos, and M. A. M. Lemes, 1980: On the stationary trough generated by the Andes. *Mon. Wea. Rev.,* **108,** 510–520.

Schubert, S. D., R. B. Rood, and J. Pfaendtner, 1993: An assimilated dataset for earth science applications. *Bull. Amer. Meteor. Soc.,* **74,** 2331–2342.

Schwerdtfeger, W., 1961: Strömungs-und temperaturfeld der freien atmosphäre uber den Anden. *Meteor. Rundsch.,* **14,** 1–6.

Shea, D. J., K. E. Trenberth, and R. W. Reynolds, 1990: A global monthly sea surface temperature climatology. NCAR Tech. Note NCAR/TN-345+STR. [Available from National Center for Atmospheric Research, P.O. Box 3000, Boulder, CO 80307-3000.]

Silva Dias, P. L., W. H. Schubert, and M. DeMaria, 1983: Large-scale response of the tropical atmosphere to transient convection. *J. Atmos. Sci.,* **40,** 2689–2707.

Ting, M., and I. M. Held, 1990: The stationary wave response to a tropical SST anomaly in an idealized GCM. *J. Atmos. Sci.,* **47,** 2546–2566.

Valdes, P. J., and B. J. Hoskins, 1989: Linear stationary wave simulations of the time-mean climatological flow. *J. Atmos. Sci.,* **46,** 2509–2527.

Vergeiner, I., and Y. Ogura, 1972: A numerical shallow-fluid model including orography with a variable grid. *J. Atmos. Sci.,* **29,** 270–284.

Virji, H., 1981: A preliminary study of summertime tropospheric circulation patterns over South America estimated from cloud winds. *Mon. Wea. Rev.,* **109,** 599–610.

Webster, P. J., 1972: Response of the tropical atmosphere to local, steady forcing. *Mon. Wea. Rev.,* **100,** 518–541.

Zheng, Q., and K.-N. Liou, 1986: Dynamic and thermodynamic influences of the Tibetan Plateau on the atmosphere in a general circulation model. *J. Atmos. Sci.,* **43,** 1340–1354.